AEDC-TR-71-191

Cy 2

RESEARCH STUDY AND EXPERIMENTAL PROGRAM TO DETERMINE THE TRANSPORT PROPERTIES OF HIGH TEMPERATURE AND HIGH DENSITY GASES

C. Carey, J. Bradshaw, and E. H. Carnevale
Panametrics, Inc.

September 1971

ARNOLD ENGINEERING DEVELOPMENT CENTER
AIR FORCE SYSTEMS COMMAND
ARNOLD AIR FORCE STATION, TENNESSEE

NOTICES

When U. S. Government drawings specifications, or other data are used for any purpose other than a definitely related Government procurement operation, the Government thereby incurs no responsibility nor any obligation whatsoever, and the fact that the Government may have formulated, furnished, or in any way supplied the said drawings, specifications, or other data, is not to be regarded by implication or otherwise, or in any manner licensing the holder or any other person or corporation, or conveying any rights or permission to manufacture, use, or sell any patented invention that may in any way be related thereto.

Qualified users may obtain copies of this report from the Defense Documentation Center.

References to named commercial products in this report are not to be considered in any sense as an endorsement of the product by the United States Air Force or the Government.

RESEARCH STUDY AND EXPERIMENTAL PROGRAM TO DETERMINE THE TRANSPORT PROPERTIES OF HIGH TEMPERATURE AND HIGH DENSITY GASES

C. Carey, J. Bradshaw, and E. H. Carnevale
Panametrics, Inc.

FOREWORD

This report was prepared by Panametrics, Inc., Waltham, Massachusetts, under U. S. Air Force Contract No. F40600-69-C-0004. This contract was initiated under Air Force Project 8951, Task No. 895102, Program Element 61102F. The work was sponsored under the direction of Arnold Engineering Development Center, Air Force Systems Command, with Lieutenant M. Buja, Project Manager.

This report covers work performed between September 1968 to September 1970.

The manuscript was released by the authors November 1970 for publication as a technical report.

The authors would like to acknowledge Charles Barber for performing measurements and for aid in data reduction and data review. The authors are grateful to Emmanuel P. Papadakis for suggesting the pulse interference technique.

The reproducibles used in the reproduction of this report were supplied by the authors.

This technical report has been reviewed and is approved.

Michael G. Buja
Captain, USAF
Research & Development Division
Directorate of Technology

Robert O. Dietz
Acting Director
Directorate of Technology

ABSTRACT

Transport property measurements with ultrasonic techniques are discussed over the entire temperature (100-15,000°K) and pressure (1-1000 atm) ranges. A chart of various techniques for the determination of transport properties in the various temperature and pressure ranges is given. Sound absorption and sound speed determinations were used to obtain thermophysical properties of argon, helium, nitrogen and air at room temperature and pressures between 1-500 atm. Several variations of pulsed ultrasonic techniques were used to obtain maximum precision in the gas property measurements. Sound speeds accurate to approximately 0.1% were obtained in all the gases. Thermal conductivity and specific heat ratios were deduced for air.

A cavity technique was developed for high accuracy (< 0.1%) viscosity, thermal conductivity and bulk viscosity determinations. Initial tests were run to proof the technique at room temperature and pressure. Sound speed, Prandtl number and viscosity measurements were made which agree with accepted values to within 1%.

TABLE OF CONTENTS

LIST OF ILLUSTRATIONS

LIST OF ILLUSTRATIONS (cont' d)

LIST OF SYMBOLS

λ	Thermal conductivity or wavelength of light
η	Viscosity or similarity parameter
η'	Bulk viscosity
D	Diffusion coefficient
σ	Effective hard sphere cross section for viscosity
χ	Enskog factor
Z_{rot}	Number of collisions necessary for rotation to come into thermal equilibrium with translation $\frac{\tau}{\tau_c}$
τ	Relaxation time
τ_c	Collisional relaxation
ρ	Density
p	Pressure
T	Temperature
v	Mass average velocity
U	Internal energy
K_T	Isothermal compressibility
β	Thermal expansion coefficient
C_v	Specific heat at constant volume (equilibrium)
C_p	Specific heat at constant pressure (equilibrium)
C_i	Internal specific heat
$\overline{C}_p, \overline{C}_v$	Complex specific heats for a single internal mode, say, rotation $\overline{C}_p = \overline{C}_v + (C_p - C_v)$ and $\overline{C}_v = C_v - \frac{j\omega\tau}{1 + j\omega\tau} C_i$

LIST OF SYMBOLS (cont' d)

γ	Specific heat ratio $\frac{C_p}{C_v}$
$\overline{\gamma}$	Complex specific heat $\overline{\gamma} = \frac{\overline{C}_p}{C_v}$
z	Compressibility factor $p = \rho\, z R T$
c	Sound speed
α	Sound attenuation coefficient
R	Gas constant
f	frequency
ω	Angular frequency $(2\pi f)$
δ	Linewidth (Hz)
ϕ	Scalar velocity potential (Eq. A.6)
k	Wave number
θ	Reduced temperature $\frac{\beta T}{\gamma - 1}$

SECTION I

INTRODUCTION

The objective of this work is the experimental determination of gas properties at high temperatures and/or pressures, with emphasis on transport properties. The immediate goals of the present work are to extend existing tabulations for immediate engineering needs and to provide long range support for theoretical work. The temperature range is $300^{\circ}K$ to $20,000^{\circ}K$, and the pressure range is 1 to 10^4 atmospheres. The principal transport properties of interest are viscosity, thermal conductivity and diffusion. In addition, consideration of other properties such as electrical conductivity, optical depth and certain thermodynamic properties are of interest.

An updated chart of the useful techniques in the temperature-pressure regions of interest, the high pressure region ($300 < t < 1000^{\circ}K$, $p < 10,000$ atm), the chemical reaction region ($1000 < t < 8000^{\circ}K$, $p < 300$ atm), and the plasma region ($800^{\circ}K > t$), as discussed in a previous report (Ref. 1), is presented in Fig. 1. Extensive ultrasonic measurements were made at Panametrics in the plasma region (Refs. 2, 3, 4). A paper is in preparation in which these measurements in nitrogen, oxygen and air are used to obtain transport properties. While there have been considerable advances in the theory of transport properties of plasmas in recent years (Refs. 5, 6), the development of new experimental techniques seems to be relatively stagnant. Some new developments with pressure and magnetic probes are in progress (Ref. 7). In addition, work is being carried out to extend transport property measurement in plasmas up to 100 atm (Ref. 8). Measurements of transport properties of plasmas are of interest for engineering of arc tunnel test facilities, magneto-hydrodynamic generators, and light source development.

The ultrasonic and Wollaston prism interferometric techniques in the shock tube were used at Panametrics in the chemical reaction region. The arc techniques do supply information in the temperature range where dissociation occurs. However, the internal inconsistency of thermal conductivity measurements from arcs is anomalously large in regions of dissociation (Refs. 9, 10, 11). The authors feel that shock tube end wall boundary layer studies with the Wollaston prism interferometer (Ref. 12), coupled with ultrasonic and molecular beam techniques (Ref. 13), will provide a firm experimental basis for transport properties of gases in the chemical reaction region. Knowledge of transport properties of gases in the temperature range $1000 < t < 8000^{\circ}K$ is a continuing engineering need for reentry and propulsion systems design and testing.

The immediate goal of the effort described below has been to develop ultrasonic techniques for the determination of thermal conductivity, viscosity, and diffusion coefficients to support theoretical work in the dense gas region. Early ultrasonic pulse measurements showed that the sum of thermal conductivity and viscosity was useful as a third independent viscosity measurement when a discrepancy between capillary and oscillating disk viscosity measurements was recognized. The ultrasonic pulse method was further developed during the past two years and applied to the measurement of transport properties of argon, nitrogen and air at elevated pressures. The sound speed measurements taken previously were spot checked with a pulse interferometric technique. Additional sound absorption measurements were made in nitrogen and argon to fill in gaps in previous measurements. In addition, the frequency range of measurements with the pulse technique was extended to 15, 21 and 27 MHz. New measurements of sound absorption and sound speed were completed in air at pressures up to ~500 atm around room temperature. Transport and thermodynamic properties of air, nitrogen and argon were derived from these measurements as described below. Further work was completed to show that a technique based on measuring the width of acoustic resonance lines in a gas filled cavity could separate the transport properties (Refs. 14, 15, 16). In addition, because the measured quantity is frequency, the cavity technique may provide the most accurate method for absolute determination of transport properties known. The resonant cavity technique was set up and measurements described below were completed which prove the basic ideas behind the measurement. The crosshatched area on Fig. 1 denotes the pressure-temperature region where the cavity technique is applicable. Measurements up to 1300°K are relatively straightforward. Extension of the technique to 2000°K with electrostatic transducers seems feasible based on our preliminary investigations.

In the future, the pulse techniques (and the schlieren interferometer) will be used for transport property measurements above 2000°K. Based on our work to date we feel the accuracy of such measurements can be kept to within 5%. The cavity technique will be used to satisfy transport property requirements below 2000°K with a precision of 0.1% or greater. With these three techniques we are in a position to take data which will extend the state-of-the-art either in the high temperature range of $3000 < T < 13,000$°K, $p < 200$ atm or the high density range $T < 2000$°K $1 < p < 1000$ atm, depending on the most pressing needs.

SECTION II

THEORY OF ULTRASONIC ABSORPTION

2.1 PHYSICAL BASIS OF ULTRASONIC TECHNIQUES

The sound wave consists of small spatial variations in pressure, temperature, flow velocity and density. These gradients cause fluxes of heat, momentum and atomic species in opposition to the reversible fluxes in the sound wave. Gradually the energy of the sound wave is lost in the form of heat. The losses eventually show up as decreases in pressure amplitude at the receive transducer. The change in sound amplitude versus distance may therefore be used to measure thermal conductivity, viscosity and diffusion coefficients.

The sound wave is ordinarily introduced by a vibrating solid surface (for an example of the opposite case see literature on the spectraphone (Refs. 17, 18)). The translational velocity of the molecules adjacent to the solid surface moves in harmony with the vibrating solid surface or transducer. In monatomic gases the fluctuations show up simply as an oscillation in pressure, temperature, particle velocity (as opposed to translational velocity), and density. In gases with internal modes of energy storage such as vibration, rotation, and electronic excitation the fluctuations in translational energy leak into the internal modes. When the translational velocity falls below the ambient value, the energy in the internal modes begins to leak out. Since the internal modes cause energy fluxes which oppose the reversible sound wave, absorption of sound energy results. Acoustic losses due to energy transfer between various molecular energy states are referred to as relaxation losses. The relaxation processes are of interest themselves in transport theory for fast relaxation effects such as rotation. Otherwise the relaxation effects must be accounted for when one desires to measure transport properties with ultrasonic techniques.

Intuitively, one should expect that a perturbation of the translational velocity of gaseous molecules travels with some suitable average of the thermal velocity of the molecules. In a monatomic gas at low pressures, the velocity of a sound wave is ~0.91 times slower than the most probable thermal velocity. The sound speed measurement, in fact, is roughly equivalent to a gas thermometer and measures the translational temperature of the gas it propagates through. One of the most attractive features of ultrasonic techniques for transport property measurements is that the temperature is automatically measured by the sound velocity.

When the temperature is known by other means the sound speed and its temperature or pressure variation are sufficient to determine all the thermodynamic properties of the gas. This is very attractive at elevated pressures.

Acoustic waves in a gas may be free waves attenuated by conversion of acoustic energy to heat within the gas, or wall waves which propagate in a thin layer of gas near a wall or discontinuity. The free waves (~1 MHz) may easily be transmitted at distances up to the order of feet by choosing a sufficiently low acoustic frequency. Therefore, the free waves are useful for reaching into hot gases above the destruction temperature of materials to determine transport properties. Wall waves decay very rapidly as they propagate away from the wall. Typical values of the attenuation length (the distance from the wall where the wall wave is attenuated to 1/e of its original value) are 10^{-2} cm at 1 kc to 10^{-4} cm at 1 MHz. The wall waves are the major source of absorption in cavities of the type employed in the acoustic resonance technique.

2.2 EXPRESSIONS RELATING TO TRANSPORT PROPERTIES, SPEED, AND ABSORPTION OF VARIOUS SOUND WAVES

The theory which relates the transport properties to the measured gradients in temperature, pressure, density or concentration in any of the conventional techniques for the determination of transport properties employs the linearized relations of fluid mechanics and certain approximate boundary conditions (Refs. 19, 20, 21). The linearization approximation is more closely fulfilled with ultrasonic techniques than conventional techniques because deviations of only 1 pt in 10^6 (pulse techniques) to 1 pt in 10^9 (cavity) of the ambient conditions are sufficient to conduct experiments.

The reduction of the linearized equations of motion to three wave equations can be carried out with no further approximations and is accomplished in Appendix A. These three wave equations describe a free wave which corresponds to the sound wave employed in the pulse technique, and two wall waves which are responsible for the major part of the absorption in the cavity technique.

The free wave propagates with a speed given to 1 pt in 10^6 by

$$c = \gamma z R T \left[1 + \frac{\rho}{z}\left(\frac{\partial z}{\partial \rho}\right)_T\right] \quad \text{cm/sec} \qquad (1)$$

and a sound absorption (in the absence of relaxation effects) equal to

$$a = \frac{1}{2\rho c} \frac{\omega^2}{c^2} \left[\frac{4}{3} \eta + \eta' + \frac{\gamma - 1}{C_p} \lambda \right] \text{ 1/cm} \qquad (2)$$

Equation (1) serves as the basis of temperature or thermodynamic property measurements. Once the compressibility factor z is known from other measurements the specific heat ratio γ or the specific heat at constant pressure C_p may be determined for sound speed and temperature determinations. The sound absorption of free waves may be used to determine any one of the three transport properties, viscosity η, bulk viscosity η', or thermal conductivity λ, once two of these quantities are known from independent measurements. At very high densities absorption of free waves is the only technique known to the authors for measurement of bulk viscosity.

The velocity and absorption of wall waves depend on either the viscosity or thermal conductivity alone. The viscous wave is generated when an acoustic field causes a velocity boundary layer near a containing wall. The sound speed (c_3) and absorption (a_3) for this wave are equal to

$$c_3 = \sqrt{\frac{2\eta\omega}{\rho}} \qquad (3)$$

$$a_3 = \sqrt{\frac{\rho\omega}{2\eta}} \qquad (4)$$

Wimilarly, the thermal wave which generated in the vicinity of a wall due to loww of heat from the temperature fluctuations in a sound field has a sound speed c_2 and absorption a_2 given by (neglecting relaxation effects on the specific heat)

$$c_2 = \sqrt{\frac{2\lambda\omega}{\rho C_v}} \qquad (5)$$

$$a_3 = \sqrt{\frac{\rho C_v \omega}{2\lambda}} \qquad (6)$$

The attenuation for both of these wall waves is very large, the wave attenuating by 1/e in one wavelength which is typically 10^{-3} cm! The viscous wave can be recognized as the usual viscoelastic wave derived in many places for liquids (Refs. 22, 23). Basically, it is the fact that

these waves depend on only viscosity or only thermal conductivity, together with the $\sqrt{\omega}$ frequency dependence (as opposed to ω^2 for free waves) which allows us to separate all the transport properties in the ultrasonic cavity technique.

The mathematical details of sound propagation are worked out in Appendix A to explicitly demonstrate that all physical effects can be rigorously accounted for. This is important to carry out because the cavity technique can apparently determine gas properties very accurately. First, we have shown in Appendix A that accurate usable expressions for acoustic losses in cavities may be obtained even after gas equation of state and relaxation effects have been included. Second, we show that the boundary value problem can be solved accurately enough to give 0.1% transport property measurement and is easily extended to provide more accurate expressions.

SECTION III

PULSE TECHNIQUES AT HIGH PRESSURE

3.1 EXPERIMENTAL SETUP FOR PULSED MEASUREMENTS AT ELEVATED PRESSURES

Various fixed path techniques were developed under the present program in an effort to obtain maximum precision in the sound absorption. The fixed path technique was chosen originally for ease of operation at elevated temperature and density ($1000^{\circ}C < T$, 1000 atm $< p$). The probe design and the high pressure cell are consistent with operating temperatures at least up to $1000^{\circ}C$. However, the major effort has been directed to high precision sound absorption at temperatures around $300^{\circ}K$. Precisions between 1 and 0.1% have been achieved during the past year.

The basic requirements for sound absorption and sound speed measurements with the pulse technique are shown in Fig. 2. A pulsed rf oscillator is used to drive a transmitter ultrasonic transducer. The sound wave is received by a similar transducer after traversing an ~1 inch gas path and is displayed on an oscilloscope. The pulse can reflect from the receiver face, the transmitter face and the resulting echo picked up after traversing three times the gas path. In practice, up to 4 echoes may be picked up before beam spreading or alignment renders the pulse unusable.

Delayed oscilloscope triggers are used to simultaneously display any two echoes or an echo and a sample of the driver pulse on the dual beam oscilloscope. An example of a display of the first transmitted pulse (the rounded trace) and the driver pulse on the dual beam oscilloscope is shown in Fig. 3. The delays are additionally used to measure transit times. As the pressure is changed a cycle of the pulse is maintained at a given point on the oscilloscope face by varying the oscilloscope trigger delay setting. The transit times are measured this way to the nearest 0.05 μsec in the present work.

The frequency of the rf pulse is determined to the nearest 5 cycles by looking at the interference between a cw signal fed into the oscilloscope in series with the rf pulse. The cw oscillator frequency is varied until (Ref. 24) stationary parallel horizontal lines appear across the oscilloscope. This means that the cw and the pulse which are incoherent interfere at constant phase points for all times displayed. Similar parallel lines will appear when the ratio of the pulse frequency to the cw frequency are

simple integers. This means that high frequencies may be measured by counting some cw subharmonics of the pulse frequency. A frequency divider was used to bring the 1-10 MHz frequencies into the range of our 1 MHz counter.

Finally, the temperature was measured with thermocouples located near each transducer. The pressure was measured with Bourdon gages, a 0-1500 psi Wallace and Tiernan gage in the low pressure range, and a 0-7500 psi Heise gage at elevated pressures. The temperature was determined to ·0.03% and pressure to better than 0.1%.

3.2 PULSE COMPARISON METHOD

In an effort to improve precision, measurements of the first transmitted pulse and the driver pulse were used to measure sound speed, density times sound speed, and sound absorption. The sound speed was measured, as mentioned above, by keeping the position of the first pulse constant on the oscilloscope face by varying the oscilloscope trigger delay. The delay was digitally set to the nearest 0.1 μsec so that the transit times are accurate to the nearest ± 0.05 μsec. This gives a precision of 0.1% in the worst case. There was enough signal-to-noise (3000-1) at the elevated pressures to accurately locate the first cycle. However, at the lower pressures, ~600 psi, the signal was too low to locate the first cycle. When a cycle was missed it showed up as a discontinuity of the transit time versus pressure curve. The transit times had to be corrected for phase shifts in the receive and transmit transducers. These corrections amount to a half period of the rf frequency: 0.15 μsec at 3 MHz and 0.05 μsec at 9 MHz.

The amplitude information obtained with the pulse comparison method may be used to measure acoustic impedance (ρc) at low frequencies and free wave sound absorption (α) at elevated frequencies. The amplitude of the first transmitted pulse is normalized by the transmitter amplitude. Thus, fluctuations in oscillator output and overall gain are normalized out. The amplitude of the first transmitted pulse is maintained within the range of one of the voltage scales of the oscilloscope. As the pressure increases less driver signal is needed because the acoustic impedance of the gas increases and the attenuation decreases. Therefore, the ratio of transmitted sound amplitude to driver pulse amplitude (V_t) increases as pressure increases.

The normalized transmitted amplitude (V_t) is given by

$$V_t = A \left(\frac{\rho c}{\rho_t c_t} \right) f(\rho c, \omega) e^{-\alpha x} \tag{7}$$

where A is a factor relating to the activity of the transducers, (ρ c) is the acoustic impedance of the gas, and $\rho_t c_t$ is the acoustic impedance of the transducer. f(ρ c, ω) is a correction which accounts for the finite transducer size and bond thicknesses. The function f(ρ c, ω), discussed in Appendix B, is close to unity. At 3 MHz the absorption is small over the pressure range of interest so that V_t is a measure of ρ c. At 9 MHz the absorption versus pressure may be determined from V_t versus pressure curves.

Photographs of 3 MHz pulses are shown in Fig. 3 at the extremes of pressure 7200 psi and 200 psi. It should be noted that the frequency and the pulse shape are not changed by the pressure variation. A plot of 3 MHz raw data in nitrogen is shown in Fig. 4. The discontinuities in the normalized amplitude versus pressure curves represent changes in oscilloscope scales used to display the driver pulse. The relative gain of the oscilloscope preamplifiers was calibrated by displaying an rf pulse of the frequency employed in data taking on two adjacent oscilloscope preamplifier voltage scales. The ratio of the readings of the same pulse on the two voltage scales was taken as a correction factor to the data in Fig. 3. This leaves only nonlinearities in the preamplifier gain and the transducer activity (the latter mainly on the transmitter side).

Photographs of the driver pulse and received pulses at 9 MHz for attenuation determinations are shown in Fig. 5. The upper photograph shows the driver pulse. The lithium niobate transducers were driven at the third harmonic to obtain 9 MHz. The structure on the driver pulse represents 3 MHz distortion in the Arenberg rf oscillator. Any three MHz component on the driver voltage which reached the receive transducer was removed by the narrow bandwidth (~500 kHz) of the receive electronics. Multiple echoes are also shown in Fig. 5. The multiple echo data were reduced to absorption to compare with the pulse comparison values as discussed below. The lower photograph shows the first received pulse and the driver pulse used for the pulse comparison attenuation determinations.

3.3 EXPERIMENTAL RESULTS WITH PULSE COMPARISON METHOD

Measurements of ρ c with 3 MHz ultrasonic waves were made in argon and nitrogen. These data have an internal consistency of ~0.1%. Additional measurements of sound absorption at 9 MHz were made in the same gases around room temperature. Sound speed determinations at 3 and 9 MHz in argon and nitrogen were also made simultaneously

with the amplitude measurements. In principle, ρc, c and absorption determinations allow both the sum of viscosity and thermal conductivity and the thermodynamic properties of the gas to be determined. However, the ρc data did not give as accurate compressibility values as can be obtained from independent PVT measurements in the temperature $\sim 300^{\circ}K$, pressure (1-500 atm) range of the present experiments (Ref. 25).

Plots of $\rho c/(\rho c)$ 300 psi are shown for argon and nitrogen in Figs. 6 and 7. The data points are consistent to about 0.1%. However, there is a 3% deviation from the "theoretical" curve at the higher pressures. The theoretical curve was obtained from compressibility data (Refs. 26, 27) and the sound speed measurement carried out in the present work. The sound speed measurements in both gases are shown in Fig. 8. The accuracy of the sound speed measurement is better than 0.1%. Therefore, the 3% discrepancy between the experimental and calculated ρc at the higher densities is probably due to imperfect reflection from the receiver face as discussed in Appendix B. These results will be discussed further in a paper in preparation.

Sound absorption measurements were made at 9 MHz by the pulse comparison technique. The results in nitrogen are plotted versus pressure in Fig. 9. Also shown are the absorption coefficients determined from the amplitude first pulse and the first echo (top Fig. 5). The first pulse-first echo data were taken for completeness. Absorption from both types of measurement shows no systematic deviations; however, the pulse comparison data is more precise in this set of data.

The pulse comparison sound absorption measurements require the ρc effects to be divided out. The ρc values used were the actual experimental results in Figs. 6 and 7. The theoretical curve in Fig. 9 is based on other transport property measurements (Ref. 28) and our rotational collision number measurements (Refs. 29, 30, 31, 32). All the results are consistent to $\sim 5\%$. The attenuation measurements by the pulse comparison technique have a precision of 1-0.1%. The question of accuracy requires further comparison with other data.

Pulse comparison measurements in argon are displayed in Fig. 10. Here, the theoretical data is that of Sengers (Ref. 33). The absorption measured in the present work is within a few percent of conventional measurements.

The pulse comparison technique seems capable of giving absorption measurements which are self-consistent to within 0.1% rms deviation. The authors feel that several items in the data reduction must be reexamined

before an absolute accuracy can be assigned to these results. First, the function $f(\rho c, \omega)$ should be reexamined. Second, the errors introduced through thermodynamic properties employed must be analyzed again, especially with regard to specific heats and sound speed. Finally, the bulk viscosity should be recalculated and uncertainties in rotational collision numbers and translational bulk viscosity estimated. The cavity measurement planned for the coming year should be useful for putting limits on the bulk loss terms. The uncertainties associated with the above factors amount to a few percent at the present time. Final calculations of these effects should be completed in the first six months of 1971.

SECTION IV

PULSE ECHO MEASUREMENTS

4.1 HIGH PRECISION PULSE ECHO FIXED PATH MEASUREMENTS

Pulse echo measurements were made with several improvements which came to light during the pulse comparison work. Acoustic nonlinearities in the gas near the transmitter and calibration of the receiver electronics were accounted for experimentally. This was done by measuring attenuation versus received amplitude and extrapolating to zero amplitude. Special care was taken to insure that the measurements were taken at the resonant frequency of the crystal or one of its harmonics. Finally, the frequency was measured with the technique discussed in Section 3.1. These improvements have eliminated most of the scatter and excess absorption noted in our previous work (Ref. 1).

Additional motivation for doing more pulse echo measurements came from a desire to obtain a check on the pulse comparison measurements. The absorption from the pulse echo method is absolute compared to the relative values obtained from the pulse comparison technique. In addition, the precision of the pulse echo measurements is about 0.1% with the current improvements. Finally, a technique based on the interference of the first pulse and first echo was used to obtain sound speeds. This technique eliminates uncertainties due to finding the first pulse and phase shifts in the transducers.

4.2 EXPERIMENTAL TECHNIQUE FOR PULSE ECHO MEASUREMENTS

The experimental apparatus for pulse echo measurements can be seen by reference to Fig. 2. A 10 to 1800 cycle acoustic pulse is initiated by driving a lithium niobate transducer with a pulsed rf oscillator as before. The acoustic wave travels through the gas and is detected by the receive transducer. However, most of the energy (~0.9999 to 0.96 in the pressure range 1-500 atm) is reflected from the face of the receive transducer. The reflected wave then reflects from the face of the transmitter and is detected after traversing the path three times. The echo is reduced in amplitude compared to the first pulse by 0.998-0.921 due to reflection losses and by $e^{-2\alpha x}$ traversing an extra two path lengths.

Measurements of frequency, pressure and temperature are carried

out as described in the pulse comparison section. The absorption is determined by measuring the amplitude of the first echo and the first pulse on a photograph of the oscilloscope face. A typical photograph is shown in the lower part of Fig. 11. The absorption is given by

$$\alpha = -\frac{\ln \frac{A_2}{A_1}}{2\ell} \tag{8}$$

where A_1 and A_2 are the amplitudes of the first pulse and the first echo (corrected for reflection losses), ℓ the probe separation, and α the absorption coefficient of the ultrasonic waves. We have adopted other improvements over previous pulse echo measurements which become necessary as accuracies of 1-0.1% are approached. We have mentioned gross heating effects due to using too much amplitude in the sound wave in previous monthlies. However, at lower amplitudes there are more subtle finite amplitude effects which simply lead to high absorption. These effects must be continually monitored for several reasons. When we double the pressure leaving the frequency and driver amplitude alone the signal which enters the gas is doubled. In addition, the average amplitude through the gas path varies through the gas. Amplitude losses of up to a factor of 100 are used to obtain accurate absorption. Therefore, in the lower useful pressure range, where the absorption is large, one must be careful of finite wave effects near the transmitter. As a result, we now check the attenuation versus amplitude at constant frequency to detect any possible finite wave effects. An example of the type of behavior observed is shown in Fig. 12. The extrapolated values of the absorption at zero voltage on the transmitter transducer is very close to the true attenuation as noted in Fig. 12.

4.3 EXPERIMENTAL TECHNIQUE FOR PULSE INTERFERENCE SOUND SPEED MEASUREMENTS

At each pressure where a pulse echo attenuation was determined, the sound speed was measured by lengthening the driver pulse width until the first pulse and the first echo overlap. The pulse and the echo interfere giving amplitudes ranging between the sum and the differences of the individual pulse amplitudes. In the upper portion of Fig. 11 the first pulse, the first echo and a region of overlap with destructive interference are shown. When the phase shift between the first pulse and the first echo in the gas is $2\pi n$, the sum of the two signals appears on the oscilloscope. On the other hand, when the phase shift across the gas path is $2\pi (n + 1/2)$ the two signals cancel. The measurement of the frequency

difference between two adjacent maxima or minima is a measure of the wavelength in the gas. Since the absorption in the high pressure cell is large, maxima and minima due to cavity resonances do not interfere with the interaction of the two signals.

In practice, the frequency difference for 10-100 maxima is swept through, starting with the rf oscillator on a frequency f_1 and finishing with frequency f_2. n minima are counted off. The frequency shift between successive minima at the average frequency $f = \frac{f_1 + f_2}{2}$ is obtained by dividing Δf by n. The frequency shift varies linearly with average frequency due to phase shifts in the transducer (Ref. 34) except at the resonance. The frequency shift between successive minima at the resonant frequency is obtained by fitting a straight line to the frequency shift versus average frequency and picking a frequency shift (Δf_o) at the transducer resonant frequency from the fit.

The sound speed is then obtained from the transducer separation (ℓ) and the measured frequency shift Δf_o from

$$c = 2\ell \Delta f_o \quad . \tag{9}$$

An example of the first sound speed measurements in helium made by this technique is shown in Fig. 13. Also shown is a line based on some interferometer measurements (Ref. 35) of sound speed in helium. The results agree well within 0.1%. The errors of the frequency determination lead to 0.05% in the individual sound speed measurements. The uncertainty in path length leads to 0.1% error in these measurements. The path length errors are systematic and do not affect the relative accuracy of the sound speed versus pressure determination.

The interference method has several advantages for sound speed determination over the pulse overlap technique used to date. First, frequency of the signal may be measured more accurately than the transit time. Second, a minimum is much easier to detect accurately than the first cycle of a pulse. Finally, the problem of calibrating or synchronizing the triggers of the first pulse and first echo channels does not arise in the interferometric technique. Since the interference technique employs a different electronic principle than the usual transit time measurement, the agreement between these two results constitutes a consistency test of the sound speed measurements.

4.4 RESULTS OF PULSE-ECHO TECHNIQUES

Sound speed was measured between 1 and 500 atm in air and argon with the pulse overlap technique. The sound speed determined by the two techniques agree with each other to within 0.1%. The sound speed versus pressure in air and argon are plotted in Fig. 14. These results compare well with independent measurements also shown in Fig. 14 (Refs. 36-40). Accurate sound speeds are important because the quantity $\frac{\gamma - 1}{C_p}$ is necessary to reduce the sound absorption to transport properties.

The major effect of thermodynamic variables occurs in the thermal conductivity terms of the sound absorption $\frac{\gamma - 1}{C_p}\lambda$. The working relations for specific heat and specific heat ratio are, respectively,

$$\gamma = (K_T)\, c^2 \tag{10}$$

$$\frac{\gamma - 1}{C_p} = \frac{(\gamma - 1)^2}{\rho c^2} \quad \frac{T}{(T^2 \beta^2)} \tag{11}$$

where the coefficient of thermal expansion β and the isothermal compressibility K_T are obtained from compressibility data and c is the measured sound speed. No independent specific heat data are used.

The major sources of error are evident in Eqs. (10) and (11). The error in γ is twice the error in sound speed (ϵ_1). Subtracting from (1) and squaring leads to a total error of $6\,\epsilon_1$ in $(\gamma - 1)^2$. The precision of the quantities $\frac{\gamma - 1}{C_p}$ therefore from Eq. (11) is $4\,\epsilon_1$. Since the error in compressibility data is about $0.1\,\epsilon_1$, the quantity which determines the accuracy of the thermodynamic inputs to the reduction of sound absorption to transport properties is therefore the sound speed.

The sound speed measurements in air are especially important because of the shortage of data on this gas. In addition, the γ and C_p deduced from the sound speed and compressibility data for reduction of

high pressure absorption measurements in air are plotted in Fig. 15. These thermodynamic data are not available elsewhere and are of value in themselves.

The sound absorption data in air were used to check the consistency of some recent tables of air, viscosity and thermal conductivity (Refs. 41, 42) versus pressure. This was accomplished by subtracting the rotational relaxation losses, and the translational bulk viscosity* losses from the total absorption to give the absorption due to transport properties. Once this quantity is obtained a consistency test of conventional measurements can be carried out. In the case of air at elevated densities the viscosity seems to be reliable, while the thermal conductivity measurements seem to have deviations up to 10%. Therefore, the contributions due to viscosity may be subtracted to provide values of λ. This comparison is shown in Fig. 16 and discussed below.

Before discussing the comparison of the measurements carried out under the present program with the correlation results of Refs. 41 and 42, the various contributions to the sound absorption should be recalled. The most interesting component of sound absorption in a gas such as air is that due to transport properties (α_c) given by

$$\frac{\rho \alpha_c}{\omega^2} = \frac{1}{2} \frac{1}{c^3} \left[\frac{4}{3} \eta + \frac{\gamma - 1}{C_p} \lambda \right] \tag{12}$$

where ρ is the density, c sound speed, C_p specific heat, γ specific heat ratio, η viscosity and λ thermal conductivity.

In addition, for a polyatomic gas such as air there is a contribution (about 20% of the total) due to rotational relaxation.

$$\frac{\rho \alpha_{rot}}{\omega^2} = \frac{1}{c} \frac{\pi}{8} \frac{\gamma - 1}{C_p} C_i \left(\frac{\eta_o}{RT} \right) Z_{rot} \tag{13}$$

This quantity can be calculated once the rotational relaxation number Z_{rot} is known. Measurements of rotational relaxation times have been carried out in a muffle tube at Panametrics and more recent theory (Refs. 41, 42)

*The temperature of the present measurements is such that vibrational relaxation is less than a 0.1% contribution even at elevated pressures.

and experiment (Refs. 43, 44) confirm the correctness of these rotational relaxation measurements. The rotational collision numbers measured at Panametrics were used to calculate the rotational bulk viscosity as outlined in a previous final report (Ref. 1).

Finally, at elevated densities there is a translational relaxation time due to multiple collisions. The bulk viscosity may be estimated from the relation

$$\eta' = \frac{4}{9} \frac{\delta^4}{m^2} (\pi m K_T)^{1/2} X \rho^2 \qquad (14)$$

where X is the Enskog factor, as discussed in Ref. 1. Since the bulk viscosity is less than 20% of the total absorption over most of the pressure range of the above experiments, the calculated corrections to the total absorption due to the bulk viscosity degrade the accuracy of the measurements by at most 3%.

The absorption values are in fair agreement with the tables of Refs. 41 and 42 as can be seen in Fig. 16. However, at the higher pressure the ultrasonic absorption measurements seem to be about 3% lower than the correlation tables. Assuming that this is mainly due to a discrepancy in thermal conductivity we eliminated the viscous losses using the viscosity tables of Ref. 41. The thermal conductivity calculated from the sound absorption measurements is less than the thermal conductivity from tables in the correlation by 6%. This may represent the errors accumulated in Ref. 42 by the fact that Lo, Carroll and Stiel were forced to use a correlation based on nitrogen measurements because existing high pressure thermal conductivity data in air was suspect.

The sound absorption in argon is plotted in Fig. 17. The consistency of this data is about 0.1%. In addition, the sound absorption calculated from Sengers' paper (Ref. 33) is in good agreement with the above measurements. The bulk viscosity is less than 20% of the total absorption and was calculated as described above.

SECTION V

CAVITY TECHNIQUE

5.1 GENERAL DESCRIPTION OF MEASUREMENT

It is generally known that sound absorption has contributions which are proportional to viscosity and thermal conductivity. The usefulness of ultrasonic pulse absorption data for providing experimental tests of transport theory in high temperature (1000-10,000°K) gases has been amply demonstrated (Refs. 1, 2, 3). However, because the effects of thermal conductivity and viscosity could not be separated and because of the difficulty of obtaining accuracies better than a few percent, the pulse technique is not competitive with conventional techniques in the lower temperature range (100-2000°K). However, a resonant cavity technique, which has provided sound absorption to within 1%, was developed in 1960 (Refs. 14, 15) and has been successfully employed at the Physikalisches Institute, Stuttgart (Refs. 16, 43) since that time. The present section describes modifications of the cavity technique and theory which potentially will provide extremely precise (<0.1%) thermal conductivity, viscosity, and other transport property measurements at temperatures below 2000°C.

The measured quantities in the acoustic cavity technique are the resonant frequencies of the cavity and frequency range over which the resonance has more than half its maximum power known as the "linewidth." The frequencies at which the resonances occur are proportional to the dimensions of the cavity and the sound speed. Therefore, in a cavity of known dimensions the resonant frequencies provide the thermodynamic properties of the gas. The linewidth on the other hand depends on the acoustic losses. This measurement in a cavity of known dimensions provides the thermal conductivity, viscosity, and other transport and relaxation properties of the gas. However, all of these properties may be separated because resonances at different frequencies depend on the various properties in independent ways.

The basic experimental reasons for the precision of the cavity measurement are the conversion of all measurements to frequency and cavity radius determinations. Using a local Loran-C station we were able to maintain a 100 kc standard oscillator to 1 pt in 10^8. In principle, this means that resonant frequency can be measured to 1 pt in 10^8 and linewidth to 1 pt in 10^6.

In order to realize some of this precision in practice the system shown in Fig. 18 was developed to measure the frequency of any part of the resonance. The procedure may be more easily understood if the resonant frequency and the linewidth are redefined in terms of phase. The phase difference between the external signal driving the cavity and and the sound field within the cavity increases by $180^{\circ}\left(\frac{\lambda}{2}\right)$ as one sweeps the frequency through a resonance. The resonant frequency is defined as the 90° phase shift point. The linewidth is the difference between the frequencies at the 45° and 135° phase points.

A phase lock amplifier has two inputs, a reference, and a signal channel. When the reference and the signal are in phase, the phase lock amplifier has a maxima. When the reference and signal channels are 90° out of phase the phase lock output is zero. First plots of phase and amplitude are made for the resonance being measured as shown in Fig. 25 for a typical cavity mode. This determines the resonant frequency to 0.3 Hz (pt in 10^5) and the location of the 45° frequency to 1 pt in 10^5. Sending the external oscillator through the phase shifter on the phase lock amplifier preset to shift the reference channel 45° a null is obtained between the external electronic oscillator and field in the cavity for the 45° point at a frequency f. A calibrated phase shift of 90° is inserted between the external oscillator and the reference channel of the phase lock amplifier. The frequency of the external oscillator driving the cavity is then increased until a null is obtained at a frequency f_2. This is the 135° point to within the precision of the original 45° phase point frequency measurement. However, because of the line symmetry, the difference between f_1 and f_2 is the true linewidth to the order of $\left(\frac{\delta}{f}\right)^3 \sim 1$ pt in 10^6 provided the 90° external phase shift is accurately calibrated. The use of a phase lock amplifier to change the phase determinations into a null allows the linewidth measurement to be carried out with a potential precision limited only by the gain of the amplifier and the harmonic distortion of the signal. When other experimental parameters such as temperature, pressure and frequency control and cavity dimension are analyzed for the experimental apparatus described below are taken into account a precision of 0.1% in the linewidth and 0.001% in the sound speed are obtained.

As discussed in the Introduction and Appendix A, the theoretical reason for the potential precision of the cavity technique is the existence of very short range thermal and viscous waves whose losses are confined to within 0.001 inches of the cavity wall. Assuming only that the Navier-Stokes equations may be linearized (good to $\sim$1 pt in 10^9 in the present case) the equations of motion of the gas reduce to a set of three wave

equations, the usual free wave, a thermal wave and a viscous wave. However, because of the short range of the thermal and viscous waves the boundary conditions on the side wall and end wall can be applied separately to an appropriate approximation. This simplification allows very accurate expressions to be derived with a minimum of labor.

5.2 SEPARATION AND MEASUREMENT OF TRANSPORT PROPERTIES

When the cavity in Fig. 18 is driven at a frequency where the waves reflected from the cavity walls reinforce, the signal on the receive transducer goes through a maxima. The pressure distribution for the second longitudinal mode is indicated by the density of dots in Fig. 18. In order to excite the cavity into a given mode the frequency of the driver is adjusted to a value close to the resonant frequency of the desired mode. Since the acoustic wavelengths are approximately the cavity dimensions in the acoustic case the resonant frequency is not unduly sensitive to cavity dimensions.

A physical insight to the separation of viscosity and thermal conductivity can be obtained by examining the particle motion in the first longitudinal and radial modes which are illustrated in Figs. 19 and 20, respectively. The longitudinal mode has particle motion parallel to the axis of the cylinder. This leads to viscous losses only on the cylindrical walls. The radial mode has particle motion in the radial direction. Thus, viscous losses are restricted to the end walls. Because of the difference in the viscous losses between the two modes, the thermal conductivity and viscosity may be obtained from measurements of two types of modes. Similar conclusions can be drawn about compound modes where the particle motion has both longitudinal and radial contributions. In addition, as illustrated in Figs. 18 and 19, the temperature distribution is different in the various modes so that the losses due to thermal conductivity also may be separated. The frequency at which the first longitudinal and first radial (f_1 and f_3, respectively) modes are excited are given in terms of the length (d) and radius (r) of the cavity as

longitudinal radial* ratio

$$f_1 = \frac{\pi}{d}\left(\frac{c}{2\pi}\right), \quad f_3 = \frac{\gamma_1}{r}\left(\frac{c}{2\pi}\right), \quad R = \frac{r}{d} = \frac{\gamma_1}{\pi}\frac{f_1}{f_3}$$

*γ_1 is the root of the equation $\frac{dj_o(\gamma_1 r)}{dr} = 0$.

The third relation may be used to eliminate the cavity length in favor of the radius and the measured frequencies.

The separation of the transport properties requires the measurement of three resonances. This is because the linewidth of any resonance depends on three independent quantities, the usual free space absorption coefficient δ_v, the longitudinal wall losses δ_{Lw}, and the radial wall losses δ_{Rw}. The measurement of the first longitudinal δ_{L1}, second longitudinal δ_{L2}, and first radial δ_{R1} mode linewidths gives three equations in δ_v, δ_{Lw}, δ_{Rw}. Alternatively, the first compound mode can replace one of the above modes with a linewidth δ_{c1} and a wall loss δ_{cw}.

Once the linewidths of the first and second longitudinal, first radial and first compound modes have been measured we have the following four relations

1st longitudinal mode

$$\delta_{L1} = \delta_v f_1^2 + \delta_{Lw} f_1^{1/2}$$

2nd longitudinal

$$\delta_{L2} = \delta_v f_2^2 + \delta_{Lw} f_2^{1/2}$$

1st radial

$$\delta_{R1} = \delta_v f_3^2 + \delta_{Lw} f_3^{1/2}$$

1st compound

$$\delta_{c1} = \delta_v f_4^2 + \delta_{cw} f_4^{1/2}$$

Any pair of these equations may be used to eliminate the free wave loss

$$\delta_v = \frac{2\pi}{\rho c^2}\left[\frac{4}{3}\eta + \eta' + \frac{\gamma - 1}{P_r}\right]$$

in favor of the measured linewidths δ_{L1}, δ_{L2}, δ_{R1} and δ_{c1}, and the measured frequencies f_1, f_2, f_3 and f_4. The bulk viscosity so determined should be accurate to better than 1% if the linewidth measurements are good to 0.01%. δ_v may then be used to eliminate the free wave losses from the measured linewidths. It is important to note that the free wave losses were chosen to be less than a 1% contribution to the linewidths. Therefore, elimination of δ_v does not introduce significant errors into wall losses.

The relations for the wall losses in terms of Prandtl number and viscosity derived by Fritsch are given in Table 1. These are the first

Table 1. Wall losses for various modes in the first approximation

radial	$\delta_{Rw} = \frac{1}{\pi r}\left(\frac{\pi \eta}{\rho}\right)^{1/2}\left[R + (1+R)\frac{\gamma-1}{P_r^{1/2}}\right]$
longitudinal	$\delta_{Lw} = \frac{1}{\pi r}\left(\frac{\pi \eta}{\rho}\right)^{1/2}\left[1 + (1+2R)\frac{\gamma-1}{P_r^{1/2}}\right]$
1st compound	$\delta_{cw} = \frac{1}{\pi r}\left(\frac{\pi \eta}{\rho}\right)^{1/2}\left[\beta^2 + 2(1-\beta^2)R + (1-2R)\frac{\gamma-1}{P_r^{1/2}}\right]$
where	$\beta = \frac{f_3}{\sqrt{f_3^2 + f_1^2}}$

approximation expressions as explained in Appendix A. The first approximation expressions are already accurate to better than 1% and have been demonstrated experimentally. In practice, the wall losses would be corrected for ρc and thermal losses to the cavity walls, line shape, and cross coupling of the wall and free waves. Preliminary examination shows these effects to be less than 0.1% in magnitude for our cavity at 1 atm and should become smaller (except ρc effects) at elevated pressures.

As an example of how the transport properties are obtained we will write down the expressions for the longitudinal and compound mode loss

$$\delta_{Lw} = \frac{1}{\pi r}\left(\frac{\pi\eta}{\rho}\right)^{1/2}\left[1 + (1+2R)\frac{\gamma - 1}{P_r^{1/2}}\right]$$

$$\delta_{cw} = \frac{1}{\pi r}\left(\frac{\pi\eta}{\rho}\right)^{1/2}\left[\beta^2 + 2(1-\beta^2)R + (1+2R)\frac{\gamma - 1}{P_r^{1/2}}\right]$$

$$\beta = \frac{f_3^2}{f_1^2 + f_3^2}$$

Dividing these two equations one obtains a relation for the Prandtl number in terms of the experimentally determined quantities δ_{Lw} and δ_{cw}

$$P_r = \left\{\frac{\left[1 - \frac{\delta_{Lw}}{\delta_{cw}}\right](\gamma - 1(1+2R))}{1 - \left[\beta^2 + 2(1-\beta^2)R\right]\frac{\delta_{Lw}}{\delta_{cw}}}\right\}^2$$

The viscosity may be obtained by subtracting these two equations, giving

$$\frac{\eta}{\rho} = \frac{\left(\delta_{cw} - \delta_{Lw}\right)^2}{\pi r^2\left[\beta^2 + 2(1-\beta^2)R - 1\right]^2}$$

Measurements of the first two longitudinal modes, the first radial mode

and the first compound mode have been demonstrated in our laboratory. The acoustic cavity technique has the unique capability of determining viscosity, thermal conductivity and relaxation effects separately in the same gas sample. In addition, the method offers potentially greater accuracy than existing techniques.

5.3 PRELIMINARY VERIFICATION OF CAVITY TECHNIQUE

Measurements intended to proof the experimental approach to gas cavity measurements in this laboratory were made in argon at 1 atm and ~300°K. The cavity employed for these measurements is shown in Fig. 21. A 0.25" diameter cylinder of pzt axially polarized material with a length corresponding to a 1.5 MHz thickness resonator was silver epoxied to a 0.0635 cm steel plate. The pzt transducer was backed with a copper cylinder. The sound generated by the transducer reached a similarly mounted transducer by a path through the gas, as well as an acoustically short circuiting path through the cavity walls (see Fig. 18). The main feature of this cavity was that all the cavity walls were flush stainless steel. The transducers are external to the cavity.

A diagram of the experimental apparatus employed for the cavity results obtained to date is shown in Fig. 18. A Loran receiver was built and through Boston College a 100 kc master oscillator which can hold 1 part in 10^8 was set up. The master oscillator frequency is locked to the Loran signal frequency using a Lissajous pattern on an oscilloscope. The master oscillator is used as the clock in a 1 MHz counter.

The frequency of the working oscillator which drives the cavity is monitored with the 1 MHz counter. The first step in making measurements consists of sweeping the frequency of the working oscillator through the frequency range of a resonance with a vacuum in the cavity. The signal through the cavity under these conditions consists of the short circuiting of sound through the cavity walls. Since this is not the desired signal, part of the output from the working oscillator is sent through a phase shifter and an attenuator which are set to cancel out the short circuiting. The cavity is then filled to the desired pressure of gas with the attenuator and phase shift set to cancel out short circuiting and the frequency range of the resonance swept through again. A trace of amplitude versus frequency such as shown in Fig. 26 (for the second longitudinal mode) is obtained. This signal represents the resonant sound field within the cavity.

The measurement of the second longitudinal, first radial and first compound modes are completed in argon at 300°K. In addition, measurements

of the first longitudinal mode were made. However, it was found that a membrane resonance in the end walls of the cavity interfered with the lower part of the frequency span of the first longitudinal mode. This is shown in Fig. 22, where a plot of the phase and amplitude versus frequency is given. The skewness of this graph shows the interference. A more revealing plot is Fig. 23, where the amplitude of the sound in the cavity is plotted as a function of phase difference between the driver and the receiver on polar paper. Ideally, this should be a circle (Ref. 44).

An examination of Fig. 23 shows that the circle is distorted at the low phase angles (next to the low frequency end of the resonance). Based on the frequency symmetry of the resonance about the center frequency one can simply fit the "good" part of the amplitude phase curve with a circle and construct the lower part of the resonance. This constructed curve is shown in Fig. 22. The linewidth of the constructed curve is close to the theoretical linewidth.

Plots of amplitude versus phase are sensitive indicators of distortion due to interfering resonances in the experimental system. Such resonances can arise from the short circuiting signal resonating in the wall or resonances in the response of the transducer. We have found membrane resonances in the cylinder end walls particularly difficult in this regard. A resonance in some member of the cavity which does not couple to the gas can be eliminated (with considerable labor) by careful vacuum measurements. However, membrane resonances contribute a phase shift to the signal across the gas path which is not present under vacuum conditions.

Polar plots of the first radial, first compound and second longitudinal modes are shown in Fig. 24. These modes show no interfering resonances in these measurements. The amplitude and phase shift versus frequency plots for these modes are plotted in Figs. 25-27. The sound speeds can be determined from the graphs to 0.01% by constructing a horizontal line through the amplitude curves and bisecting it to find the resonant frequency. However, the dimensions of the cavity used were only held to 0.05%. (A cavity has been supplied at no charge to us by Federal Products, a division of Esterline Corporation, with dimensions held to 20 μin.

The linewidths could be determined from the graphs to about 1%. However, when actual data is taken the center frequency is approximately located with graphs such as those given and the 45^{o} frequencies are determined from direct counter readings of frequency at $\pm 45^{o}$. As pointed out before, the symmetry of the phase shift versus

frequency relation means that errors in linewidth due to errors in center frequency are small. However, to minimize frequency drift, etc., the $\pm 45^{o}$ points should be measured as rapidly as possible. An automatic method for simultaneously measuring the $\pm 45^{o}$ points to be described later, has been developed.

The data taken is summarized in Table 2. Sound speeds derived from all three modes agree with calculated values and other measurements to 0.1%. Thermal conductivity and viscosity values were derived from the second longitudinal and first compound modes. These are compared to accepted values in Table 2. The values measured with the cavity technique agree with the accepted values to well within 1%. No special attempt was made to control temperature ($\pm$ 0.5°C) or pressure ($\pm$ 10 mm) in the above work. However, the data taken indicates that the technique is basically sound.

Table 2. Transport properties measured with cavity technique

	1st Compound Linewidth Hz	2nd Longitudinal Linewidth Hz	Prandtl No.	Viscosity Poise
Present work	198.5	185.5	0.660	2.23
Michels Ref. 33	-	-	0.669	2.25

SECTION VI

SUMMARY

The acoustic pulse techniques have been thoroughly explored for transport and thermodynamic property determination. The pulse techniques have the unique capability of reaching into a hot gas ($2000 < T < 15,000$) and can make valuable contribution to thermophysical properties at these temperatures. Pulse techniques were further developed during the present program to provide specific acoustic impedance (ρc) and attenuation to precisions of 1-0.1% from amplitude measurements. Using these techniques measurements were carried out in argon, helium, nitrogen and air at temperatures around 300°C and pressures up to 500 atm. Data reduction of air measurements was carried to completion. Thermal conductivity and specific heat ratio of air up to ~500 atm are reported. Measurements in the other gases agree with attenuation, acoustic impedance and sound speed calculated from independent data. Further analysis of this data for publication is in progress.

A new technique capable of providing highly precise thermal conductivity and viscosity determinations was developed. This technique has been employed for several years to make 1% sound absorption determinations. We have extended the theory so that it is suitable to deduce 0.01% thermal conductivity and viscosity values from linewidth measurements. In addition, we have modified the cavity and transducer in a way more suitable for high pressure transport property determinations. Initial Prandtl number and viscosity values taken in this apparatus show that the technique is working as designed.

REFERENCES

1. Carey, C., Carnevale, E. H., Uva, S. and Marshall, T., "Experimental Determination of Gas Properties at High Temperatures and/or Pressures," AEDC-TR-69-78 (March 1969).

2. Carnevale, E. H., Larson, G., Lynnworth, L. C., Carey, C., Panaro, M. and Marshall, T., "Experimental Determination of Transport Properties of High Temperature Gases," NASA-CR-789 (1967).

3. Uva, S., "Ultrasonic Propagation in High Temperature Gases and Plasmas," Ph. D. Thesis, Boston College (1968).

4. Carnevale, E. H., Lynnworth, L. C. and Larson, G. S., "Ultrasonic Determination of Transport Properties of Monatomic Gases at High Temperatures," J. Chem. Phys. 46, 3040 (1967).

5. Sandler, S. I., Miller, E. J. and Mason, E. A., "Transport Properties of Partially Ionized Argon," Proc. 5th Symposium on Thermophysical Properties, ASME, New York (1970).

6. Devoto, R. S., "Transport Coefficients of Partially Ionized Hydrogen," J. Plasma Phys. 2, 617 (1968).

7. Schreiber, P. W., Hunter, A. M. II and Benedetto, K. R., "Nitrogen Plasma Viscosity Measurements," in Proc. 5th Symposium on Thermophysical Properties, ASME, New York (1970).

8. Bouder, U. H. and Bartelheimer, D. L., "On the Determination of Plasma Properties at Very High Pressures," Proc. 5th Symposium on Thermophysical Properties, ASME, New York (1970).

9. Asinovsky, E. I. and Shabaskov, V. I., "Experimental Study of the Electrical and Thermal Conductivity of Air Plasma," 7, 203 (1969).

10. Morris, J. and Rudis, R., "Evaluation of High Temperature Gas Transport Properties," Final Report Avco SSD-0414-67-PR.

11. Morris, J. C., Rudis, R. P. and Yos, J. M., "Measurements of Electrical and Thermal Conductivity of Hydrogen, Nitrogen, and Argon at High Temperature," in Selected Papers Presented at the High Pressure Arc Symposium, A. M. Hunter, ed., ARL-70-0135 (1970).

REFERENCES (cont' d)

12. Smeets, G., "Determination of Hot Gas Thermal Conductivity By Shock Tube Experiments," Proc. of the 5th International Shock Tube Symposium, 28-30 April 1965, AD 484 600.

13. Amdur, I. and Mason, E. A., "Intermolecular Forces and High Temperature Properties," in Proc. 5th Symposium on Thermophysical Properties, ASME, New York (1970).

14. Fritsche, L., "Präzisionsmessung Der Klassischen Schallabsorption mit Hilfe Des Zylinderresonators I," Acoustica 10 (1966).

15. Fritsche, L., "Theorie Des Acoustischen Zylinderresonators Unter Berücksichtigung Der Schallanregung II," Acoustica 10, 199 (1960).

16. Roesler, H., "Der Zylinderresonator Fur Präzisionsmessungen Der Schallabsorption in Gasen," Acoustica 17, 73 (1966).

17. Kerr, E. L. and Atwood, J. C., "The Laser Illuminated Absorptivity Spectrophone: A Method for Measurement of Weak Absorptivity in Gases at Laser Wavelengths," App. Optics 7, 915 (1968).

18. Kaiser, R., "On the Theory of the Spectrophone," Can. Jour. Phys. 37, 1499 (1959).

19. Newell, G. F., "Theory of Oscillation Type Viscomerters V: Disk Oscillating Between Fixed Plates," Zamp 10, 160-174 (1959); (see also Zamp 8, 433, 1957).

20. Giddings, J. G., Kao, J. T. F. and Kobayashi, K., "Development of a High Pressure Capillary-Tube Viscometer and Its Application to Methane, Propane and Their Mixtures in the Gaseous and Liquid Regions," J. Chem. Phys. 45, 578 (1966).

21. Tsederberg, N. V., Thermal Conductivity of Gases and Liquids, Chap. I., MIT Press (1965).

22. Lindsay, R. B., Mechanical Radiation, McGraw-Hill, p. 351 (1960).

23. Simmons, J. H. and Macedo, P. M., "High Temperature Shear Ultrasonic Interferometer Using Sensitive Phase Lock Detection System," JASA 43, 1295-1301 (1968).

REFERENCES (cont' d)

24. Papadakis, E. P., "Elastic Wave Velocities in Cube Textured Copper Sheet," Trans. Met. Soc. AIME 236, 1609 (1966).

25. Robertson, S. L., Babb, S. E. and Scott, G. J., "Isotherms of Argon to 10,000 bars and 400°C," J. Chem. Phys. 50, 2160 (1969).

26. Robertson, S. L. and Babb, S. E., "Isotherms of Nitrogen to 400°C and 10,000 bars," J. Chem. Phys. 50, 4560 (1969).

27. Bender, E., Equations of State Exactly Representing the Phase Behavior of Pure Substances, in 5th Symposium on Thermophysical Properties, ASME (1970).

28. Carnevale, E. H., Carey, C., Marshall, T and Uva, S., "Experimental Determination of Gas Properties at High Temperatures and/or Pressures," AEDC-TR-68-105 (1968).

29. Carnevale, E. H., Carey, C. and Larson, G., "Ultrasonic Determination of Rotational Collision Numbers and Vibrational Relaxation Times of Polyatomic Gases at High Temperatures," J. Chem. Phys. 47, 2829 (1967).

30. Lordi, J. A., "Rotational Relaxation In Nonpolar Diatomic Gases," Ph. D. Thesis, New York University (May 1968). (See also Phys. Fluids 13, 291 (1970).)

31. Brau, C. A. and Jonkman, R. M., "Classical Theory of Rotational Relaxation in Diatomic Gases," J. Chem. Phys. 52, 447 (1970).

32. Healy, R. N. and Storvick, T. S., "Rotational Collision Number and Eucken Factors From Thermal Transpiration Measurements," J. Chem. Phys. 50, 1419 (1969).

33. Michels, A., Sengers, J. V. and Van DeKlondert, L. J. M., "The Thermal Conductivity of Argon at Elevated Densities," Physica 29, 149-150 (1963).

34. Truell, R., Elbaum, C. and Chick, B. B., Ultrasonic Methods in Solid State Physics, Academic Press, New York (1969).

REFERENCES (cont'd)

35. Gamnon, B. E. and Douslin, B. R., A System for Measuring the Velocity of Sound in Compressed Fluids and Its Application to Helium Between -175 and 150°C, in Proc. 5th Symposium on Thermophysical Properties (C. F. Bunilla, ed.), ASME (1970).

36. El-Hakeen, A. S., "Velocity of Sound in Nitrogen and Argon at High Pressures," J. Chem. Phys. 42, 3132-3133 (1965).

37. Van Herbeck, A., Van Dael, W. and Greuendon, W., "Measurements on the Velocity of Sound in Argon Under High Pressure," Physica 25, 640-644 (1959).

38. Lestz, S. S. and Grove, R. N., "Second Virial Coefficients from Acoustic Isotherms," J. Chem. Phys. 43, 883-885 (1965).

39. Hilsenrath, J., Beckett, C. W., Benedict, W. S., Fano, L., Hoge, H. J., Masi, J. F., Nuttall, R. L., Touloukian, Y. S. and Woolley, H. W., Tables of Thermodynamic and Transport Properties of Air, Argon, Carbon Dioxide, Carbon Monoxide, Hydrogen, Nitrogen, and Steam, Pergamon Press, New York (1960).

40. Bradley, R. S., High Pressure Physics and Chemistry, Vol. I, Academic Press, London, 72-90 (1963).

41. Lo, H. Y., Carroll, D. L. and Stiel, L. I., "Viscosity of Gaseous Air at Moderate and High Pressure," J. Chem. and Eng. Data 11, 540 (1966).

42. Carroll, D. L., Lo, H. Y. and Stiel, L. I., "Thermal Conductivity of Gaseous Air at Moderate and High Pressures," J. Chem. and Eng. Data 13, 53 (1968).

43. Bauer, H. J. and Schotter, R., "Collisional Transfer of Vibrational Energy From Nitrogen and Methane to Carbon Dioxide Molecules," J. Chem. Phys. 51, 3261-3270 (1969).

44. Slater, J. C., Microwave Electronics, Van Nostrand and Co., New York (1950).

APPENDIX A

DERIVATION OF EXPRESSIONS DESCRIBING SOUND PROPAGATION IN A CAVITY

EQUIVALENCE OF WAVE EQUATIONS AND LINEARIZED NAVIER-STOKES

The basic equations which define the thermal conductivity and viscosity are the conservation of energy, momentum and mass. In addition, the equation of state and an internal energy relation must be specified to completely determine the flow of a fluid subject to given boundary conditions. The linearized equations of motion for a pure dense gas including real gas equation of state and relaxation of internal modes are

energy
$$\frac{\partial U}{\partial t} + p_o \nabla \cdot \bar{v} - \lambda \nabla^2 T = 0 \qquad \text{(A. 1)}$$

momentum
$$\rho_o \frac{\partial \bar{v}}{\partial t} + \nabla p - \eta \nabla^2 \bar{v} + (\eta' + \frac{1}{3}\eta)\nabla \cdot (\nabla \bar{v}) = 0 \qquad \text{(A. 2)}$$

mass
$$\frac{\partial p}{\partial t} + \rho_o \nabla \cdot \bar{v} = 0 \qquad \text{(A. 3)}$$

equation of state
$$p = z\rho RT \qquad \text{(A. 4)}$$

internal energy
$$\frac{\partial U}{\partial t} = \left(\frac{\partial U}{\partial \rho}\right)_T \frac{\partial \rho}{\partial t} + \bar{C}_v \frac{\partial T}{\partial t} \qquad \text{(A. 5)}$$

Here the internal energy U is defined in terms of a complex specific heat $\bar{C}_p$ and the translational temperature T. One could define the temperature statistically (Ref. A. 1) and have relaxation effects show up in the bulk viscosity η' or use the nonequilibrium thermodynamics formalism (Ref. A. 2). However, we chose to define a complex specific heat for brevity which leads to identical answers. Methods for obtaining complex specific heats are worked out elsewhere (Refs. A. 3, A. 4). We will simply carry $\bar{C}_v$ through the calculation to show how relaxation effects enter the absorption and velocity relations.

Equations (A. 1-A. 5) constitute 5 equations in the 5 unknowns: internal energy U, pressure p, velocity $\bar{v}$, translational temperature T,

and density ρ. With appropriate boundary conditions expressions for the flow field in terms of the thermal conductivity λ, viscosity η, volume viscosity* η', and specific heat can be derived. The most common way to derive the desired expressions for attenuation and sound speed is to assume solutions of the type $e^{-i(k-i\alpha)x}$ exist and by substitution into (A. 1-A. 5) derive values for k and α (Ref. A. 4). However, Fritsche (Ref. 5) was able to reduce the above five equations to a set of four wave equations with no further approximations. Proceeding in this way allows all the physical phenomena to be evaluated easily. In addition, boundary conditions may be applied to the resulting wave equations in a standard way.

The velocity may be separated into a rotational and irrotational part in the usual manner

$$v = \nabla\phi + \nabla \times \bar{H}_3 \tag{A.6}$$

where ϕ is the scalar potential and $\bar{H}_3$ the vector velocity potential. The momentum equation (A. 2) then becomes

$$\nabla\Phi + \nabla \times \left(\frac{\partial \bar{H}_3}{\partial t} - \frac{\eta}{\rho_o} \nabla^2 \bar{H}_3 \right) = 0 \tag{A.7}$$

with the new scalar potential Φ defined as

$$\Phi = \frac{\partial\phi}{\partial t} - \left(\frac{\eta + \eta'}{\rho_o} \right) \nabla^2 \phi + \frac{p}{\rho_o} \tag{A.8}$$

The wave equation for viscous waves which propagate near a wall separates immediately from (A. 7) giving

$$\nabla^2 \bar{H}_3 + k_3^2 \bar{H}_3 = 0 \tag{A.9}$$

The wave number for these waves is

$$k_3 = (1 + i) \sqrt{\frac{\rho\omega}{2\eta}} \tag{A.10}$$

*The volume viscosity in the present formalism includes only many body contributions.

The velocity pressure and density may be eliminated from the scalar part of the momentum and energy equation (A. 8) using the equation of state

$$\frac{\partial}{\partial t}\left(\frac{p}{\rho_o}\right) = \frac{1}{\rho_o^{\,2} K_T}\frac{\partial \rho}{\partial t} + \frac{\beta}{\rho_o K_T}\frac{\partial T}{\partial t} \tag{A. 11}$$

where

$$K_T = \frac{1}{p_o}\,\frac{1}{\left[1 + \frac{\rho_o}{z}\left(\frac{\partial z}{\partial \rho}\right)_T\right]} \tag{A. 12}$$

$$\beta = \frac{1}{T_o}\,\frac{1 + \frac{T_o}{z}\left(\frac{\partial z}{\partial T}\right)_\rho}{\frac{\rho_o}{z}\left(\frac{\partial z}{\partial \rho}\right)_T}\,, \tag{A. 13}$$

the internal energy equation (A. 5), the conservation of mass (A. 3) and the definition of the velocity potential (A. 6). The resulting equations are with no approximations

$$\nabla^2 \Phi = 0 \tag{A. 14}$$

$$i\omega\frac{c_o^{\,2}}{\gamma}\theta + \left[\frac{c_o^{\,2}}{\gamma} - i\omega\left(\frac{4}{3}\eta + \eta'\right)\right]\nabla^2\phi + \omega^2\phi - i\omega\phi = 0 \tag{A. 15}$$

$$\frac{\lambda}{\rho C_v}\nabla^2\theta + i\omega\theta - \frac{C_p - C_v}{\overline{C}_v}\nabla^2\phi = 0 \tag{A. 16}$$

where θ is $\frac{\beta T}{\gamma - 1}$, and the thermodynamic identities

$$\frac{1}{\rho K_T} = \frac{c_o^{\,2}}{\gamma} \quad \text{and} \quad \left[p_o - \rho_o\left(\frac{\partial U}{\partial \rho}\right)_T\right] = \frac{C_p - C_v}{\beta} \tag{A. 17}$$

have been used.

Each of the equations (A. 11), (A. 12) and (A. 13) resemble wave equations; therefore, it makes sense to see if the variables Φ, ϕ and θ can be replaced to three quantities H_ℓ ($\ell = 0, 1, 2$) which obey wave equations

$$\nabla^2 H_\ell + k_\ell H_\ell = 0 \tag{A. 18}$$

A simple linear expansion in the H_ℓ is the most obvious route to try

$$\phi = \sum_0^3 H_\ell \tag{A. 19}$$

$$\theta = \sum_0^3 a_\ell H_\ell \tag{A. 20}$$

$$\Phi = \sum_0^3 b_\ell H_\ell \tag{A. 21}$$

If values of k_ℓ, a_ℓ and b_ℓ can be found then the set of wave equations (A. 14) may be used to apply the boundary conditions of the particular problem at hand.

Substitution of (A. 19-A. 21) in (A. 14-A. 16) provides the desired quantities. Substitution in (A. 11) shows that if $b_\ell \neq 0$ $k_\ell = 0$ and the first wave equation is immediately

$$\nabla^2 H_0 = 0 \text{ and } k_o = 0 \tag{A. 22}$$

The remaining cases are for $b_\ell = 0$ $k_\ell \neq 0$. After substitution of (A. 19) through (A. 21) into (A. 15) and (A. 16) one obtains for a_ℓ

$$a_\ell = \frac{C_p - C_v}{\overline{C}_v} \quad \frac{k_\ell^2}{i\omega - \frac{\lambda}{\rho \overline{C}_v} k_\ell^2} \tag{A. 23}$$

and for k_ℓ^2 the quadratic equation

$$\frac{\lambda}{\rho \overline{C}_v}\left[\frac{c_o^2}{\gamma} + \frac{\left(\frac{4}{3}\eta + \eta'\right)}{i\omega\rho_o}\right] k_\ell^4 - \left[\frac{\overline{\gamma}}{\gamma}\frac{c_o^2}{\omega^2} + \frac{\frac{4}{3}\eta + \eta'}{i\omega\rho_o} + \frac{\lambda}{i\omega}\frac{\lambda'}{\rho_o C_v}\right] k_\ell^2 + 1 = 0 \tag{A. 24}$$

Finally, after much laborious algebra and approximation, the two remaining wave numbers follow from (A. 24)

$$k_1^2 = \frac{\omega^2}{c^2}\left[1 - i\frac{\omega}{\rho_o c^2}\left(\frac{4}{3}\eta + \eta' + (\bar{\gamma} - 1)\frac{\bar{C}_p}{\bar{C}_p}\frac{\lambda}{C_p}\right)\right] \tag{A.25}$$

$$k_2^2 = i\omega\bar{\gamma}\frac{\rho\bar{C}_v}{\lambda}\left[1 - i\frac{\omega}{c^2}\frac{\bar{\gamma} - 1}{\bar{\gamma}}\left(\frac{4}{3}\eta + \eta' + \frac{\bar{\gamma}}{\bar{\gamma} - 1}\frac{\lambda}{\rho\bar{C}_v}\right)\right] \tag{A.26}$$

The basic equations of motion (A. 1-A. 5) have been reduced to three wave equations with wave numbers given by (A. 9, A. 25) and (A. 26). These wave numbers are explicit functions of transport properties, relaxation times, thermodynamic quantities and frequency. The approximations which lead to (A. 25) and (A. 26) from (A. 24) are not necessary but lead to errors of only one part in 10^{12} in k_1 and k_2. In addition to one part in 10^6, the second terms in (A. 25) and (A. 26) may be neglected. These terms represent the coupling between wall waves and free waves that one might expect physically.

The waves, H_1, H_2 and H_3, related to velocity pressure and temperature through the potentials defined in Eqs. (A. 6-A. 8) and the relations (A. 19-A. 21). Expressions for $v(H_1, H_2, H_3)$, $p(H_1, H_2)$ and $T(H_1, H_2)$ can be obtained from the relations (A. 6-A. 8) and (A. 17-A. 19), in terms of the known wave numbers k_1, k_2, k_3 and the quantities a_1 and a_2. These relations transform the boundary condition on pressure, temperature and flow velocity into conditions on the solutions H_1, H_2 and H_3.

Following the procedure for separation of variables one might expect the first wave equation

$$\nabla H_1 + k_1^2 H_1 = 0 \tag{A.27}$$

to have solutions of the sort

$$H_1 = \sum_{p=0}^{\infty} A_p^{(1)} J_o(\gamma_p^{(1)} r)\, e^{i k_p^{(1)} z} \tag{A.28}$$

where $\gamma_p^{(1)}$ and $k_p^{(1)}$ are to be determined from the boundary conditions and are required to satisfy

$$\gamma_p^{(1)2} + k_p^{(1)2} = k_1^{(2)}. \tag{A.29}$$

One might expect to proceed in a similar fashion with the separation of the wave equations for H_2 and H_3. However, in general, in acoustic resonators, because H_1, H_2 and H_3 are coupled, the solutions of separated wave equations cannot be made to fulfill all the boundary conditions on the end walls and side walls simultaneously. Physical insight provides a unique separation of the wave equations which allows the boundary to be approximately satisfied. For instance, the separation for H_3 may be made in the form

$$H_2 = \sum_{p=0}^{\infty} A_p^{(2)} J_o(\gamma_p^{(2)} r)\, e^{ik_p^{(1)} z} + \sum_{p=0}^{\infty} B_p^{(2)} J_o(\gamma_p^{(1)} r)\, e^{ik_p^{(2)} z} \qquad \text{(A. 30)}$$

where the first term represents a thermal wall wave along the side wall of the resonator excited by the H_1 wave $e^{ik_p^{(1)} z}$. And the second term represents a thermal wave on the end wall of the resonator driven by the free wave $J_o(\gamma_p^{(1)} r)$. A similar separation can be effected for the viscous waves (H_3).

In order for these waves to be solutions to the wave equations for H_2 and H_3

$$k_p^{(1)2} + \gamma_p^{(2)2} = k_2^2 \qquad \text{(A. 31)}$$

and

$$k_p^{(2)2} + \gamma_1^{(1)2} = k_2^2 \qquad \text{(A. 32)}$$

must hold.

Fritsch showed that $k_p^{(1)} \sim k_1$ and $\gamma_p^{(1)} \sim \gamma_p$ (k_1 or γ_1 are the wave parameters for the zero viscosity thermal conductivity case). This leads to $\gamma_p^{(2)2} \sim k_2^2$ and similar results for $\gamma_p^{(3)}$ and $k_p^{(3)}$. Therefore, the first term in Eq. (A. 30) is small at any distance from the side wall of the cavity ($\frac{1}{e}$ at $r \simeq 0.001$). Similarly, the second term is small at any distance from the end wall. This is because the wall waves fall off rapidly as we leave the wall. An excellent approximation may therefore be obtained by applying the boundary conditions on the side walls of the cavity neglecting the second terms in (A. 30). This gives traveling waves in both directions including the viscous and thermal waves. A reflection coefficient for these waves may be obtained at the end walls using only the second terms in Eq. (A. 30), which satisfy the end wall boundary conditions.

A complete solution can be built up in the above fashion leading to the expressions for linewidth and resonant frequency given in the text. These expressions neglect stress and temperature fluctuations in the wall and imperfect reflection from the end walls. In addition, some algebraic approximations are made in the linewidth expressions. However, the first order solution is already good to 0.1% over the range of operating conditions anticipated, $200 < T < 1000^{\circ}C$, $p < 500$ atm. Corrections to the linewidth can be derived by a simple perturbation method to correct the measured linewidth to within 0.01% of the first order expressions. These corrections will be presented in a later report.

REFERENCES

A. 1 Monchick L., Yun, K. S. and Mason, E. A., "Formal Kinetic Theory of Transport Phenomena in Polyatomic Gas Mixtures," J. Chem. Phys. 39, 654 (1963).

A. 2 deGroot, S. R. and Masur, P., Non-Equilibrium Thermodynamics, North Holland Pub. Co., Amsterdam (1963) Chap. X11.

A. 3 Herzfeld, K. F. and Litovitz, T. A., Absorption and Dispersion of Ultrasonic Waves, Academic Press, New York (1959).

A. 4 Carnevale, E. H., Larson, G., Lynnworth, L. C., Carey, C., Panaro, M. and Marshall, T., "Experimental Determination of Transport Properties of High Temperature Gases," NASA CR-789 (1967).

A. 5 Fritsche, L., "Theorie Des Acoustischen Zylinderresonators Unter Berücksichtigung Der Schallanregung II," Acoustica 10, 199 (1960).

APPENDIX B

TRANSDUCER ANALYSIS FOR PULSE TECHNIQUE

The transducers employed in pulse sound speed and attenuation measurements are the key to obtainable precision and temperature range. The transducer needs to be sufficiently damped to provide pulses which do not interfere with each other. In addition, the pulses must reach their steady state value in a reasonable time (~20 μsec). The range of frequencies at which the transducer has usable output in the neighborhood of a resonant frequency increases as the damping increases. However, output decreases with more damping. The ability to resonate at harmonics also decreases as damping is increased. The transducer mounting is designed as a compromise between these effects. In addition, the transducer, bonding and backup materials must be consistent with the highest desired working temperature. Finally, alignment and parallelism of all parts are important if accurate estimation of phase shifts and interference in the transducer body are required.

The transducer employed in all the measurements reported is shown in detail in Fig. 1B. The acoustically active elements shown in the lower part of Fig. 1B are the most important. A lithium niobate piezoelectric crystal is bonded with silver epoxy to a zinc backup. The zinc provides a sufficient sound absorption and ρc match to the lithium niobate transducer to provide adequate damping. The rise time of the lithium niobate transducers with zinc backup plates is about 30 cycles at their 3 MHz fundamental frequency.

The active transducer elements are bonded into the supporting stainless steel transducer body with high temperature cement as shown in the upper part of Fig. 1B. The front electrode is made by coating the transducer assembly with silver epoxy and grinding the layer to about 0.003" thick. The transducer body slips into a mount which maintains alignment and makes electrical contact.

The waves reflected from the interfaces of the various layers in the transducer interfere causing delays and apparent attenuation of the sound waves. For instance, the first pulse entering the transducer is delayed by the transit time in the front silver layer. In addition, if the first half cycle is not used to determine the arrival time, interference of the waves reflected from the transducer interface causes an additional delay of up to $1/2\lambda$. Finally, waves which have entered the transducer can come out again and interfere with the signal in the gas. Each reflection leads to addition of this "reradiated" signal and leads to a modification

of the signal in the gas. When the transducer is operated at resonance the reradiated signal is in phase with the echo. However, when the transducer is operated off resonance the attenuation may appear to increase with the magnitude of the difference between the operating frequency and the resonant frequency.

Finally, when using a transducer such as shown in Fig. 1B for pulse comparison determinations of ρc and attenuation the correct reflection and transmission coefficients must be used. For instance, the relation between the sound wave incident on the receive transducer and the sound wave in the transducer involves the sum of signals which are multiply reflected within the front silver epoxy layer. To a lesser extent, the signal which leaves the transducer enters the backup layer and the bond, subsequently reflecting into the transducer, also contributes to the transducer response.

We will calculate the transmission coefficient of the front layer of the receive transducer. The signal enters the layer from the gas with a reduction of amplitude T_{o1} given by

$$T_{o1} = \frac{\rho_o c_o}{\rho_1 c_1 + \rho_o c_o} \sim \frac{\rho_o c_o}{\rho_1 c_1} \tag{B. 1}$$

where $\rho_o c_o$ is the acoustic impedance of the gas and $\rho_1 c_1$ is the acoustic impedance of the layer.

The wave in the layer then reflects from the transducer-front layer interface. Some of the incident energy, namely

$$\psi_t = T_{o1} T_{12} e^{ik_1 \ell} \psi_o \tag{B. 2}$$

where ψ_o is the incident signal in the gas, ψ_t the signal in the transducer and T_{12} is the transmission coefficient at the transducer-front layer interface

$$T_{12} = \frac{\rho_1 c_1}{\rho_1 c_1 + \rho_2 c_2} \tag{B. 3}$$

k_1 is the wave number $\left(\frac{2\pi}{\lambda}\right)$ in the front layer.

Considering the multiple reflections of a signal in the front layer as leaking some signal into the transducer at each reflection we can add up the total signals entering the transducer. For a train of n pulses this is

$$\psi_t = \psi_o T_{o1} T_{12} \left[1 + R_{12} e^{ik_1 \ell} \frac{1 - (R_{12} R_{10})^n e^{2ink_1 \ell}}{1 - R_{12} R_{10} e^{2ik_1 \ell}} \right] \qquad \text{(B. 4)}$$

where the reflection coefficients at the front layer-transducer interface and the front layer-gas interface are

$$R_{12} = \frac{\rho_1 c_1 - \rho_2 c_2}{\rho_1 c_1 + \rho_2 c_2} \qquad \text{(B. 5)}$$

and

$$R_{10} = \frac{\rho_1 c_1 - \rho_o c_o}{\rho_o c_o + \rho_1 c_1} \sim 1. \qquad \text{(B. 6)}$$

The important thing to note is that the signal in the transducer depends on the frequencies (via $k_1 = \frac{\omega}{c_1}$) and the thickness of various layers. In addition, the dependence on the acoustic impedance of the gas is much more complex than the simple $\frac{\rho_o c_o}{\rho_1 c_1}$ dependence used to explain the principle of the measurement in the text.

Fortunately, the magnitude of R_{10} is approximately 1 for a gas and $R_{12} \sim 0.5$. Therefore, the complex terms added to 1 in Eq. (B. 4) are small. However, one has to be careful because when the front layer is $\sim 1/4\lambda$ thick and the acoustic impedance of the layer is the geometric mean of the acoustic impedance of the transducer and the gas the signal in the gas is entirely transmitted into the transducer!

The important transducer parameters are listed in Table 1B. The thickness of the various elements of the transducers are given. A short calculation shows that the front layers are not an even multiple of $\frac{\lambda}{4}$ for either of the transducers at the operating frequencies. In addition, the

Table 1B. Transducer mounting and parameters

Transducer Parameters		
Thickness (cm)	Receive Transducer	Transmit Transducer
Front silver layer	0.0071	0.0081
Lithium niobate	0.106	0.106
Bond	0.005	0.005
Zinc	0.635	0.635

Probe separation 2.4809 ± 0.0019 cm

Material Parameters (300°K)

		$LiNbO_3$	Zinc	Silver Epoxy	N_2 1 atm	10	100	500
Sound speed (longitudinal	cm/μsec	0.652	0.421	0.1909	0.0353	0.354	3.80	
						x 10^{-3}		
Wavelength	3 MHz	0.217	0.140	0.0636				
	9 MHz	0.0724	0.0463	0.0212				
Acoustic impedance	gm/μsec cm^2	3.025	3.00	0.5011	0.0402	0.404	4.31	22.6
						x 10^{-3}		

acoustic impedance of the front layers never reaches the geometric mean of the acoustic impedance of the gas and the transducer in the pressure range of these experiments. In fact, for nitrogen

$$\sqrt{\rho_2 c_2 \rho_o c_o} < 0.261$$

A complete description of transducer corrections is beyond the scope of this report. However, the information in Table 1B defines all the necessary parameters. Transducer characteristics were also measured using the frequency behavior of the transducer. These results will be reported more completely in later papers on the pulse techniques.

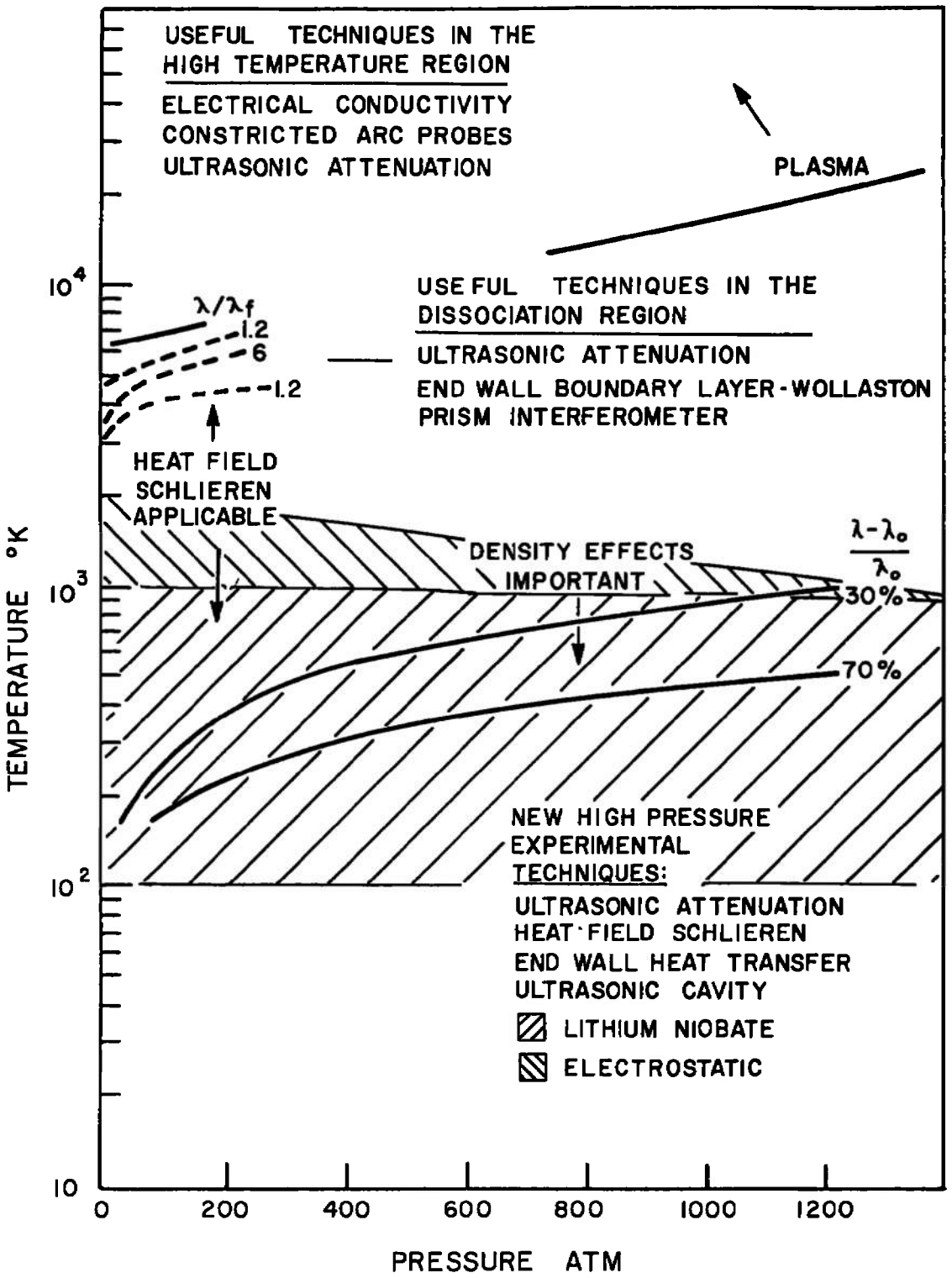

Fig. 1. Useful pressure-temperature ranges of various techniques of transport property determination

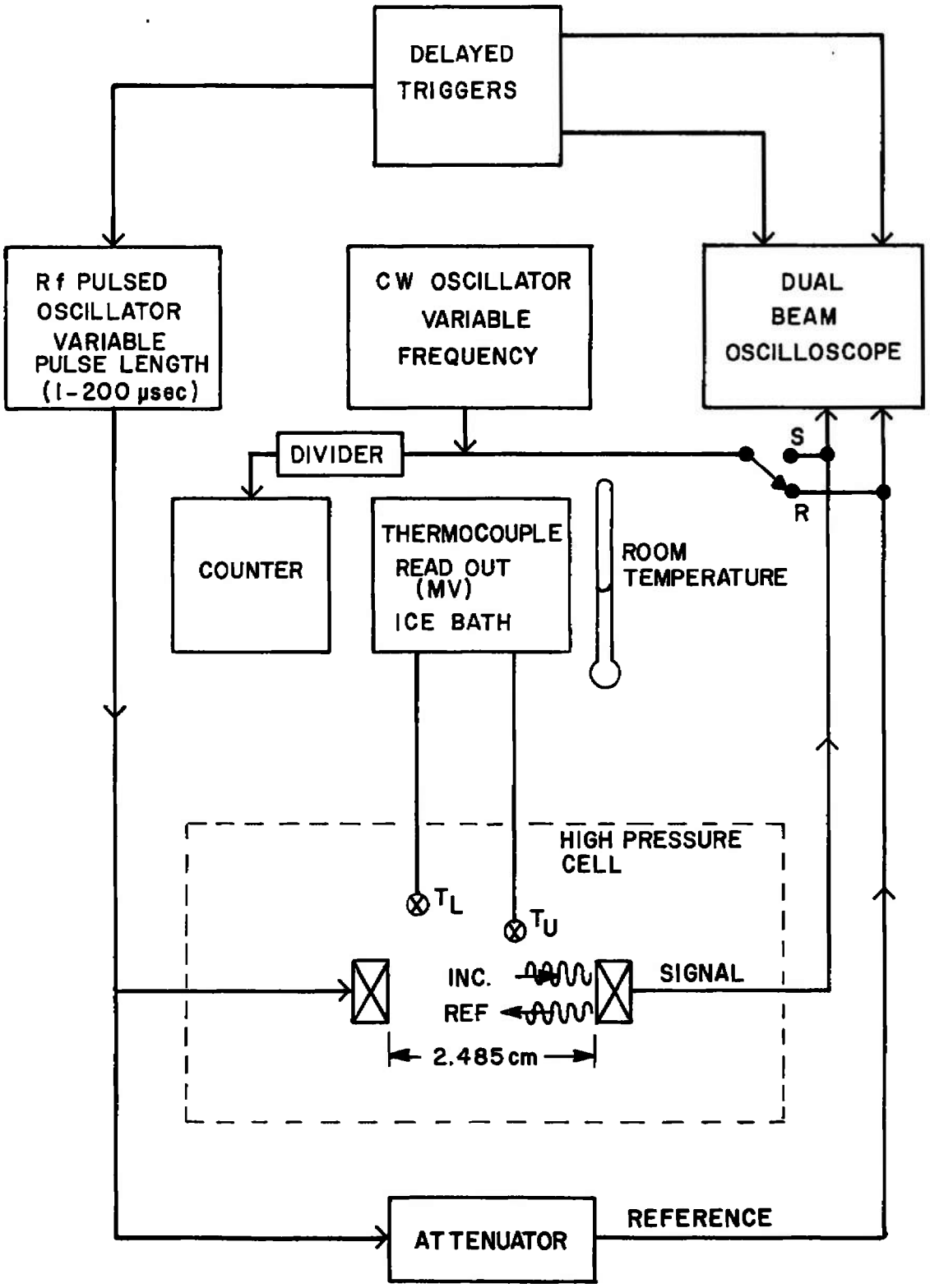

Fig. 2. Schematic of experimental apparatus for pulse techniques

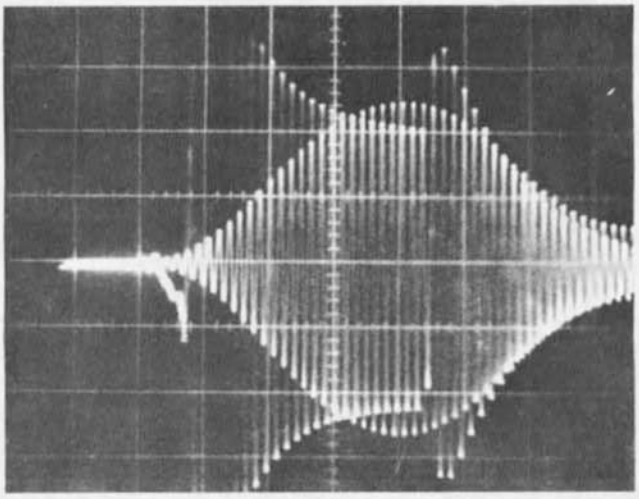

3 MHz Driver Pulse and Transmitted Pulse p = 7200 psi V_o = 8.1 Volts

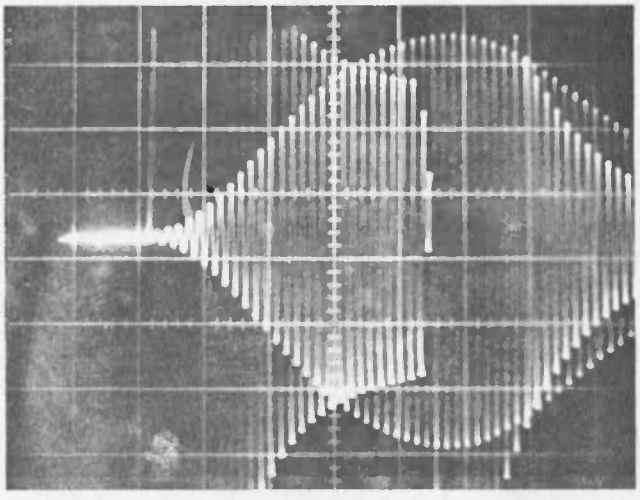

3 MHz Driver Pulse and Transmitted Pulse p = 200 psi V_o = 420 Volts

Fig. 3. 3 MHz relative amplitude acoustic impedance traces

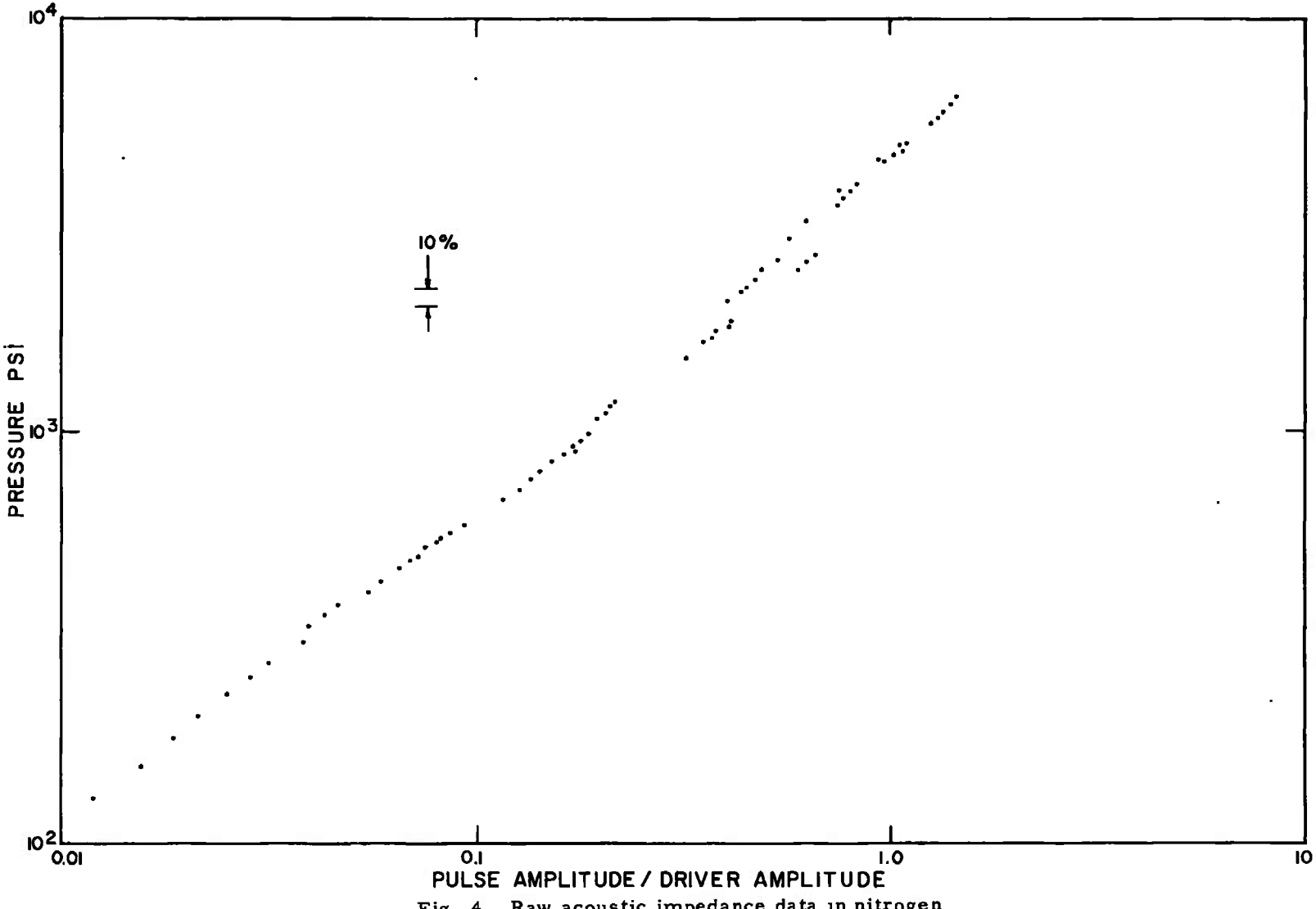

Fig. 4. Raw acoustic impedance data in nitrogen

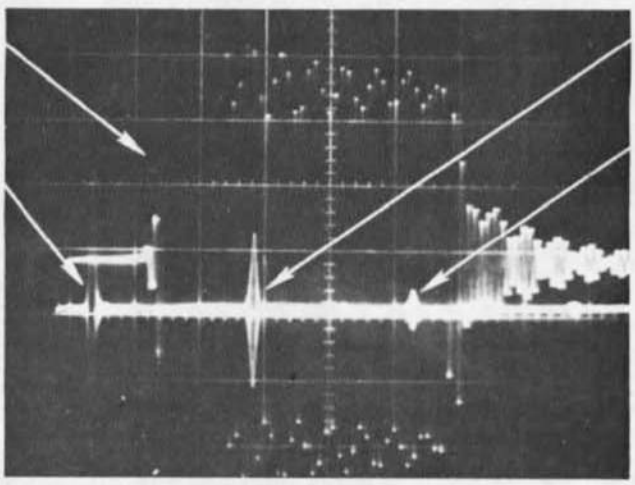

9 MHz driver pulse and multiple echo

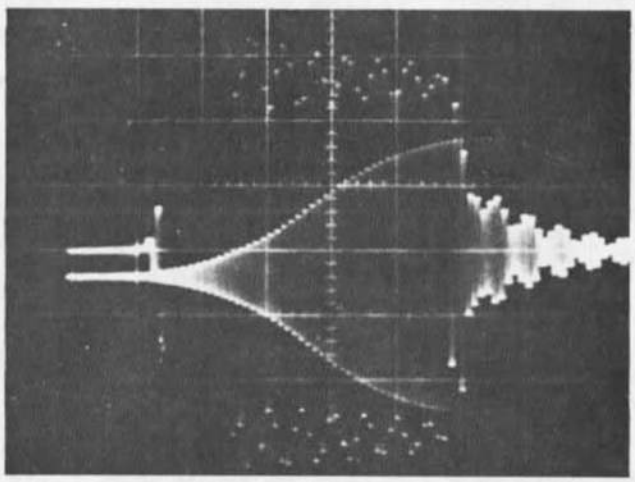

9 MHz transmitted pulse and driver pulse

Fig. 5. 9 MHz relative amplitude acoustic attenuation traces

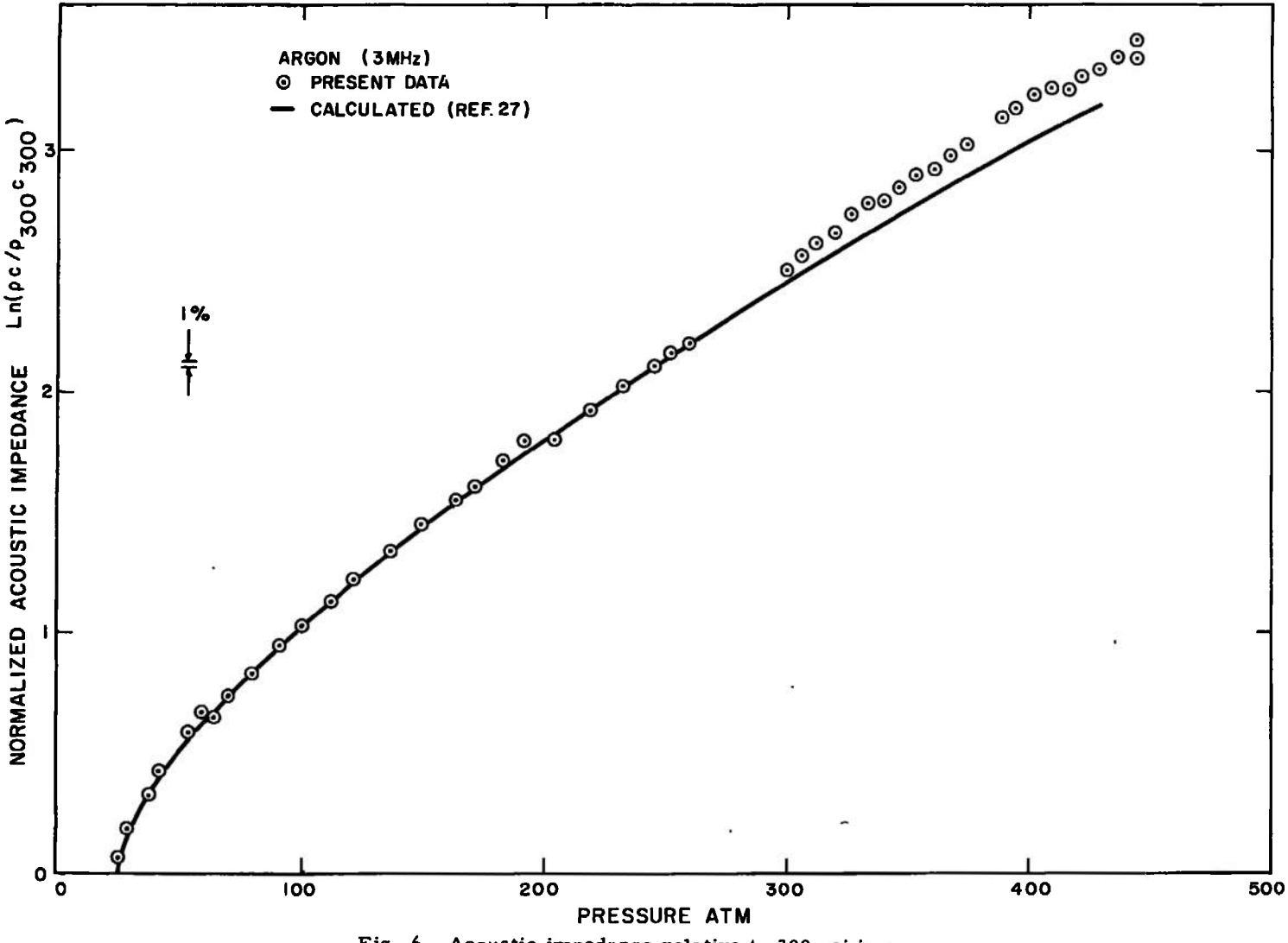

Fig. 6. Acoustic impedance relative to 300 psi in argon

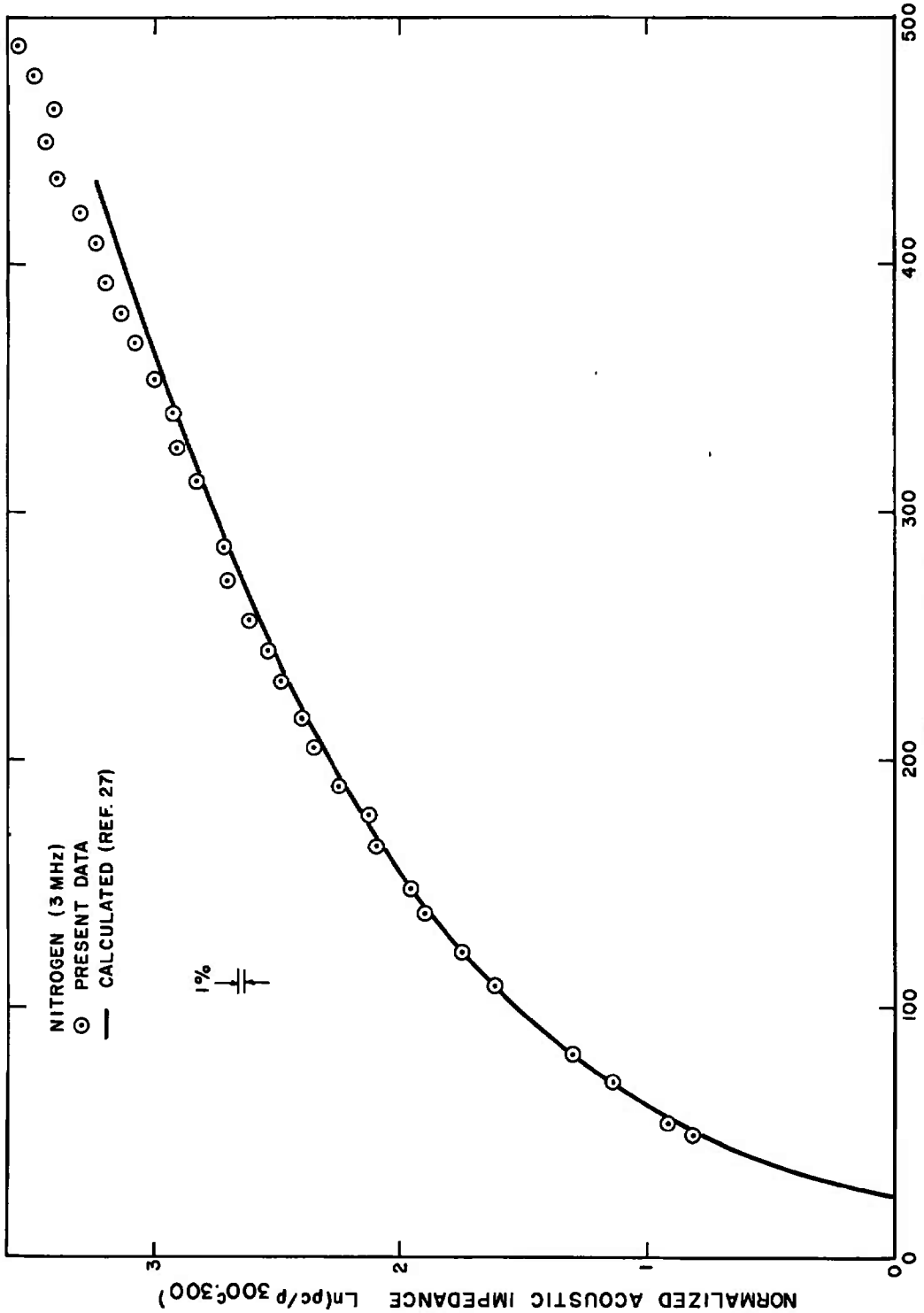

Fig. 7. Acoustic impedance relative to 300 psi in nitrogen

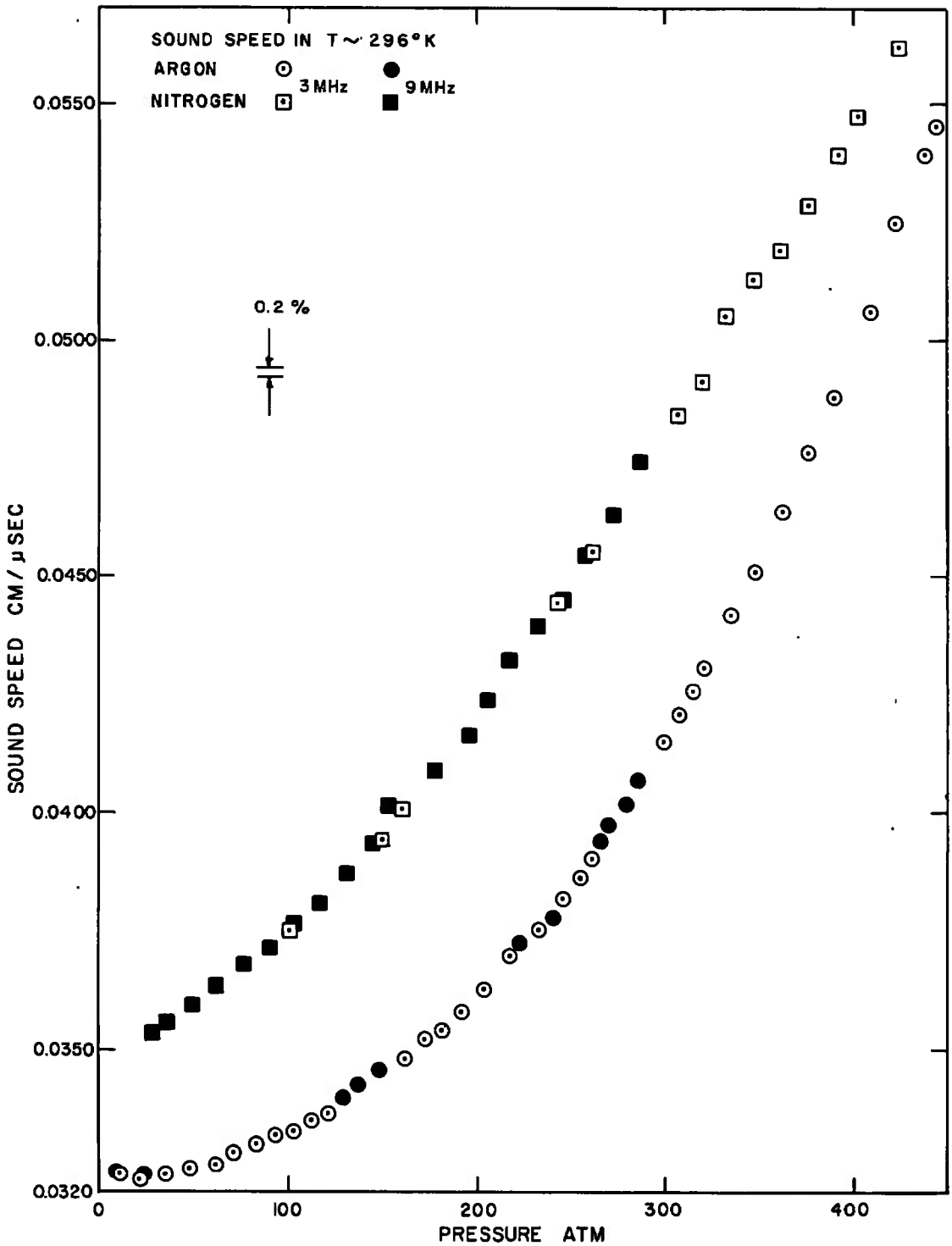

Fig. 8. Sound speed versus pressure in argon and nitrogen

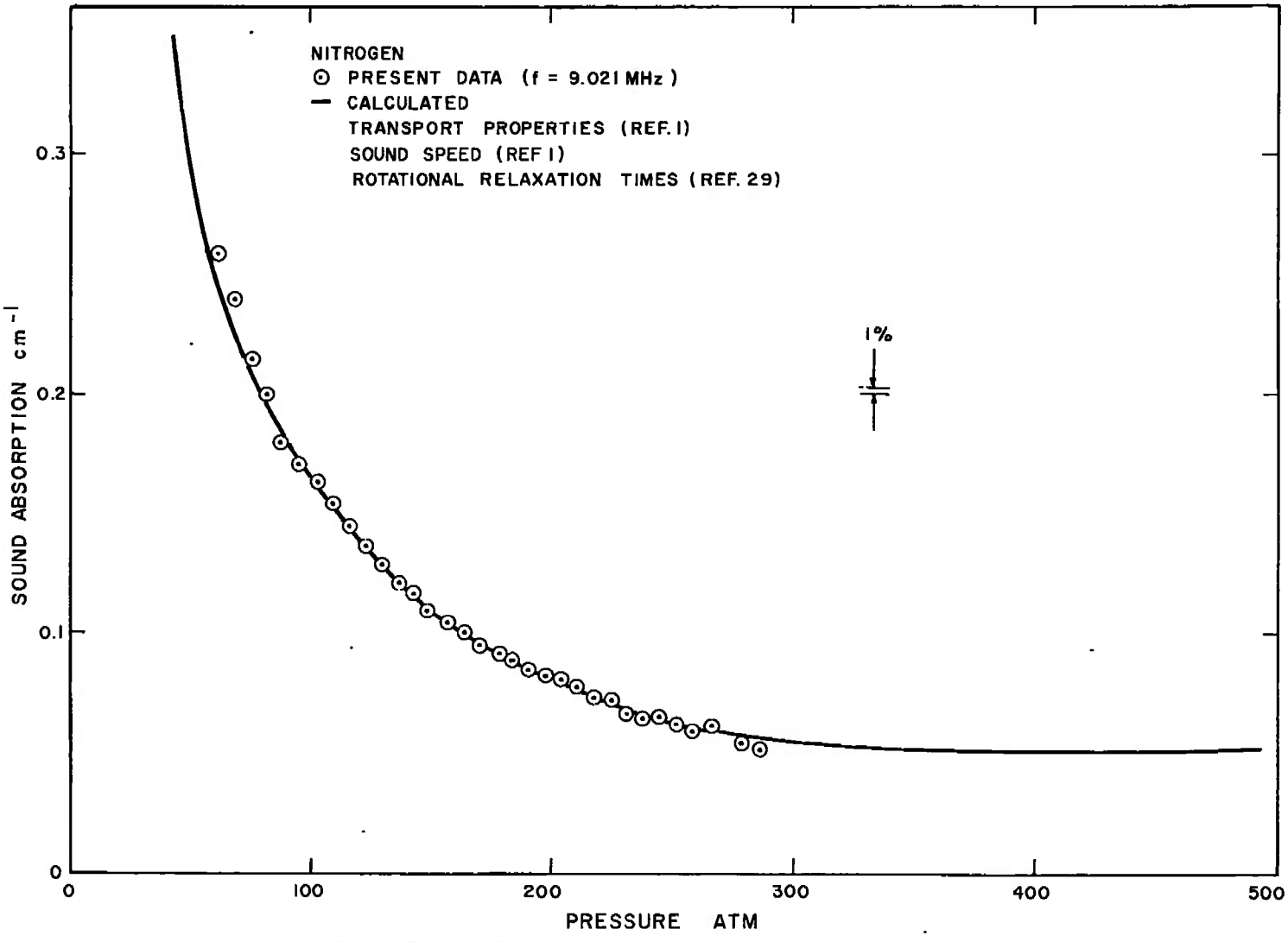

Fig. 9. Sound absorption in nitrogen by the pulse comparison technique

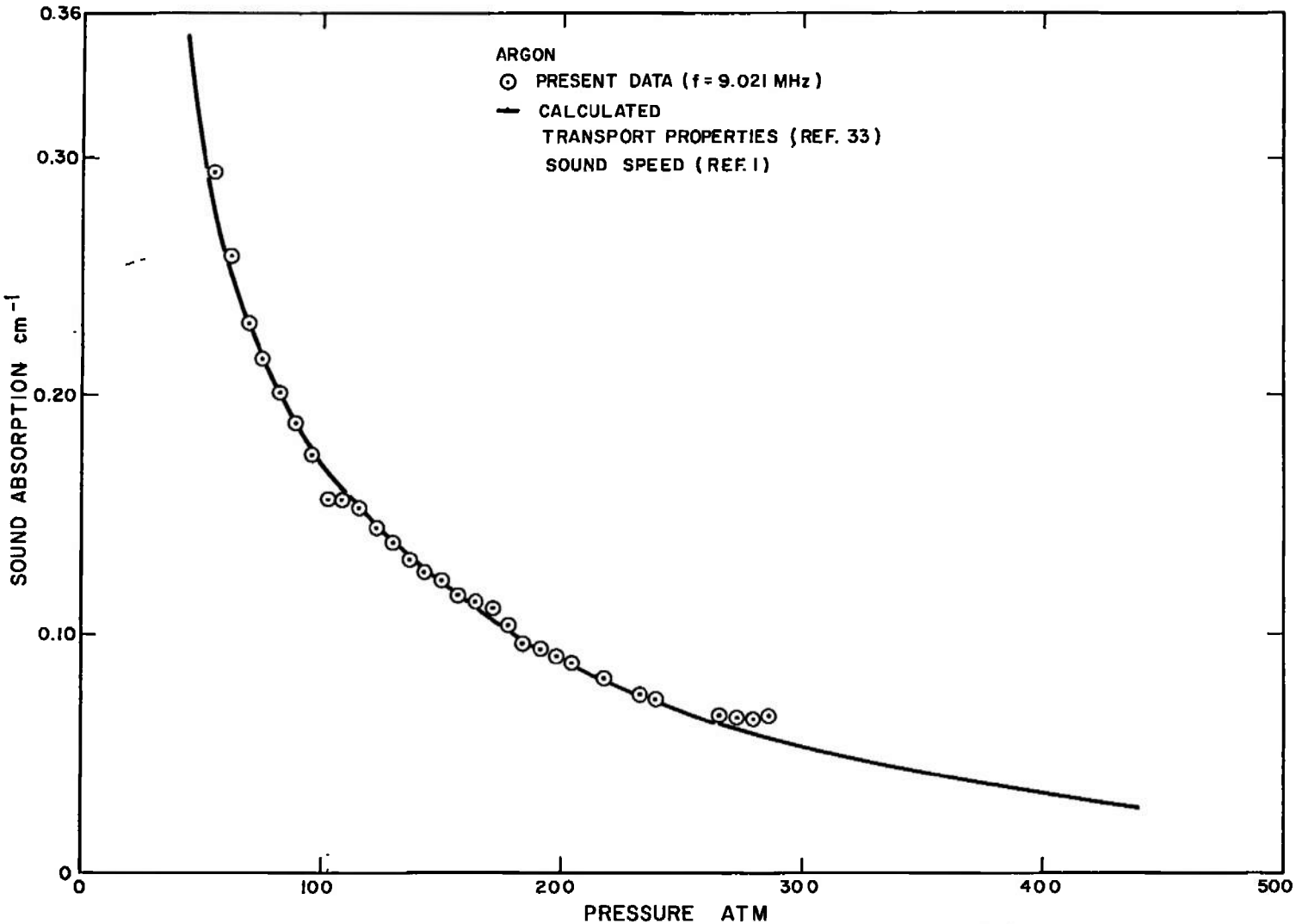

Fig. 10. Sound absorption in argon by the pulse comparison technique

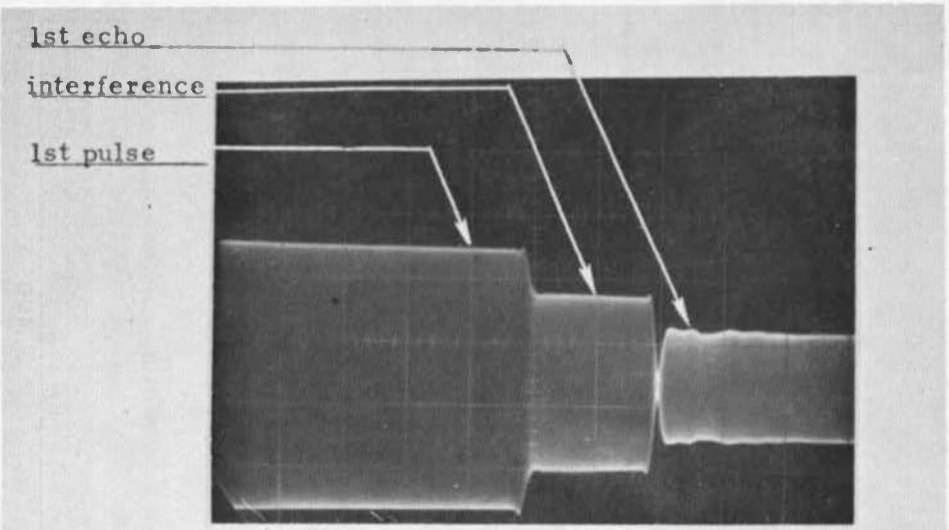

Sound speed by interference of 1st pulse and 1st echo

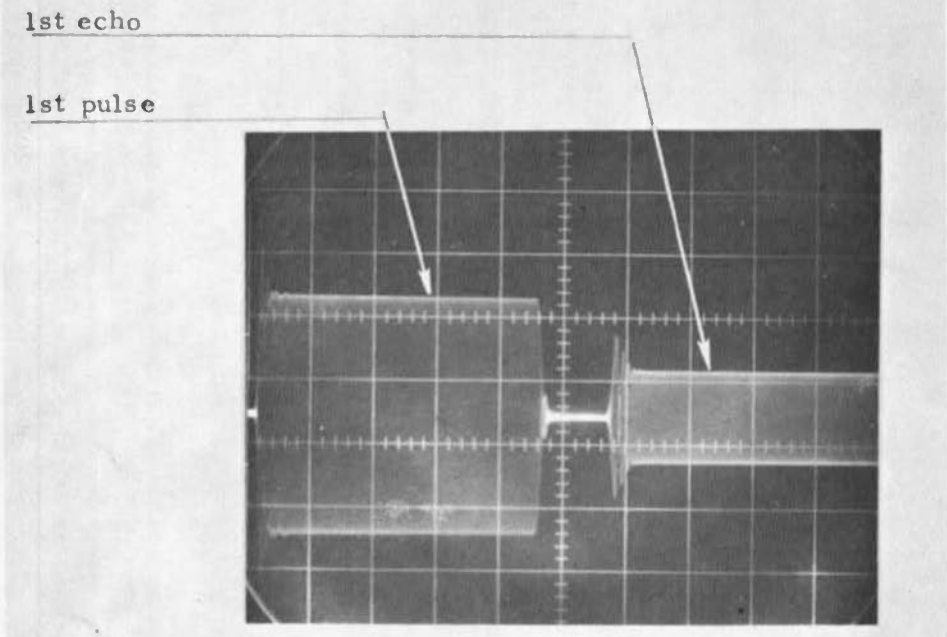

Attenuation trace

Fig. 11. 9 MHz through transmission multiple echo and pulse-echo interference traces.

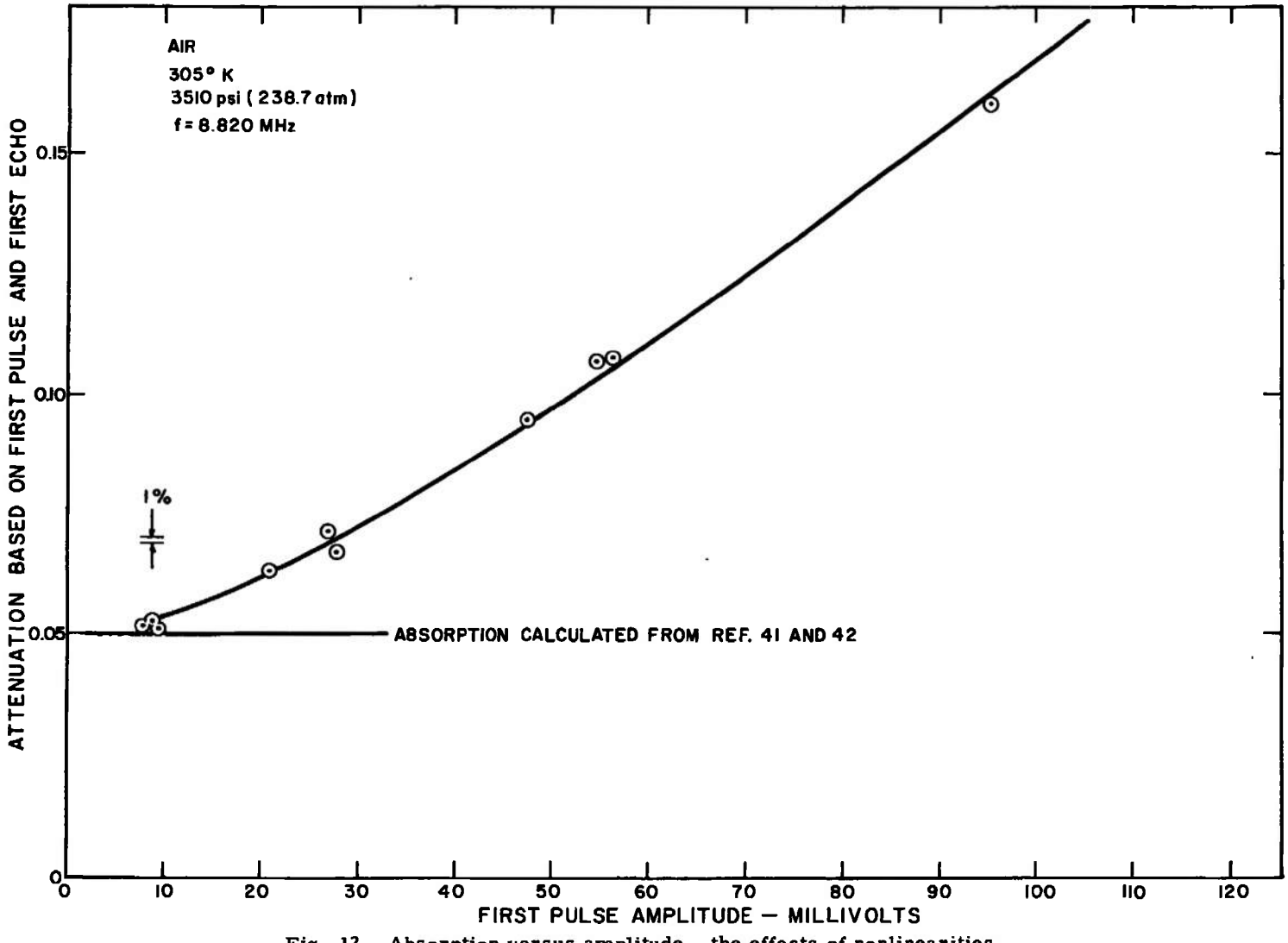

Fig. 12. Absorption versus amplitude - the effects of nonlinearities

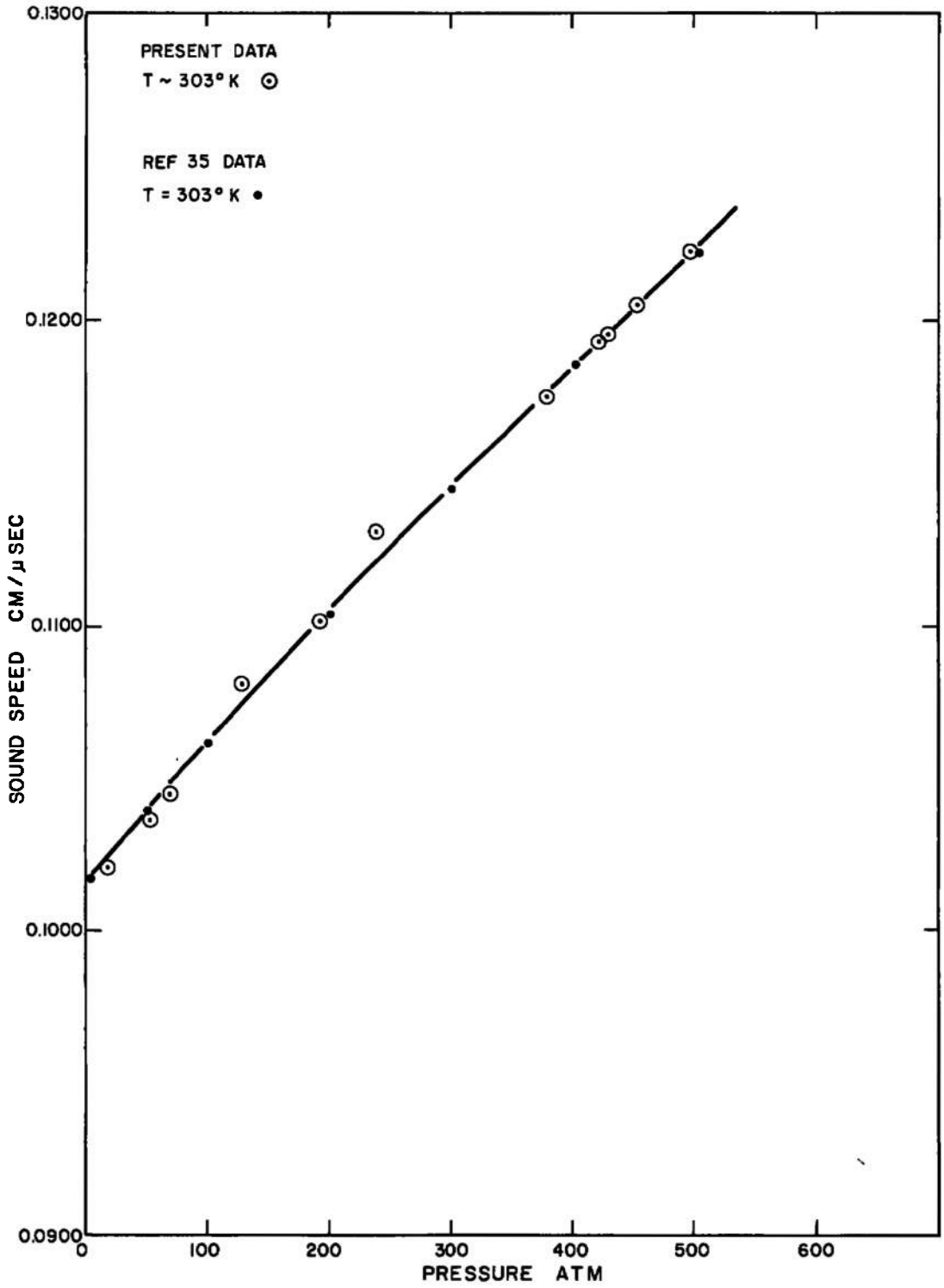

Fig. 13. Sound speed versus pressure in helium by the pulse interference technique

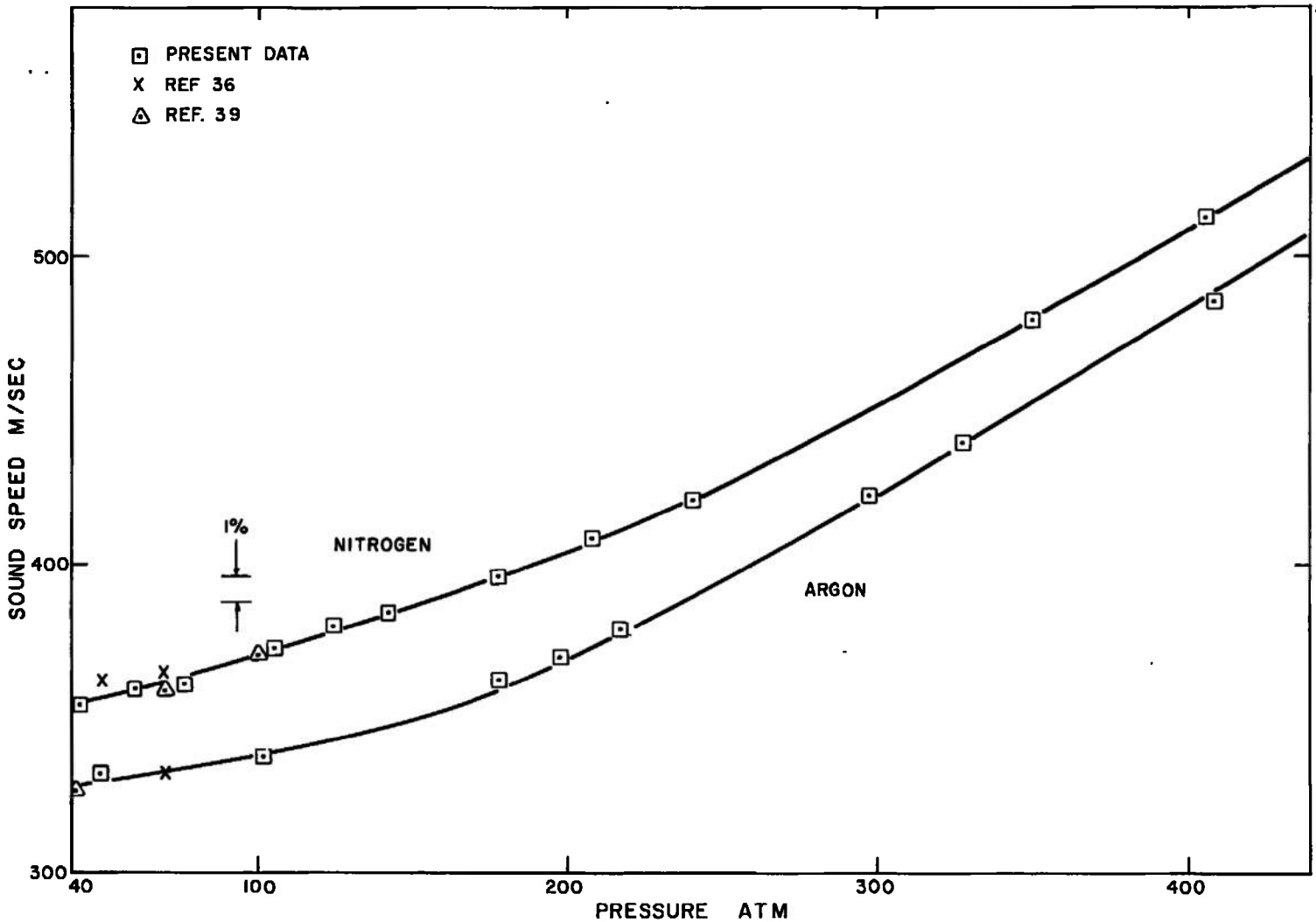

Fig. 14. Sound speed versus pressure in air and argon by the pulse interference technique

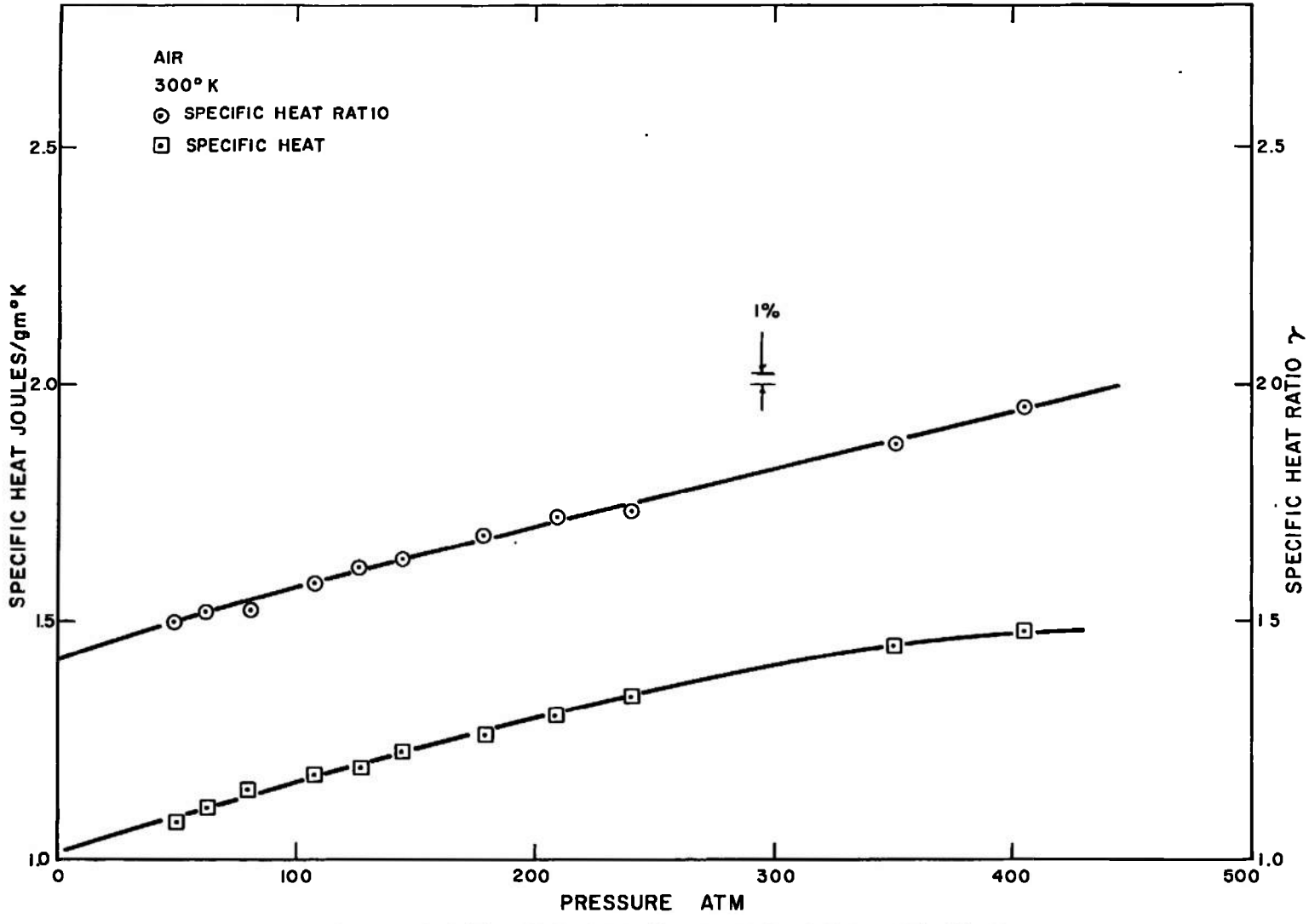

Fig. 15. Specific heat and specific heat ratio versus pressure in air

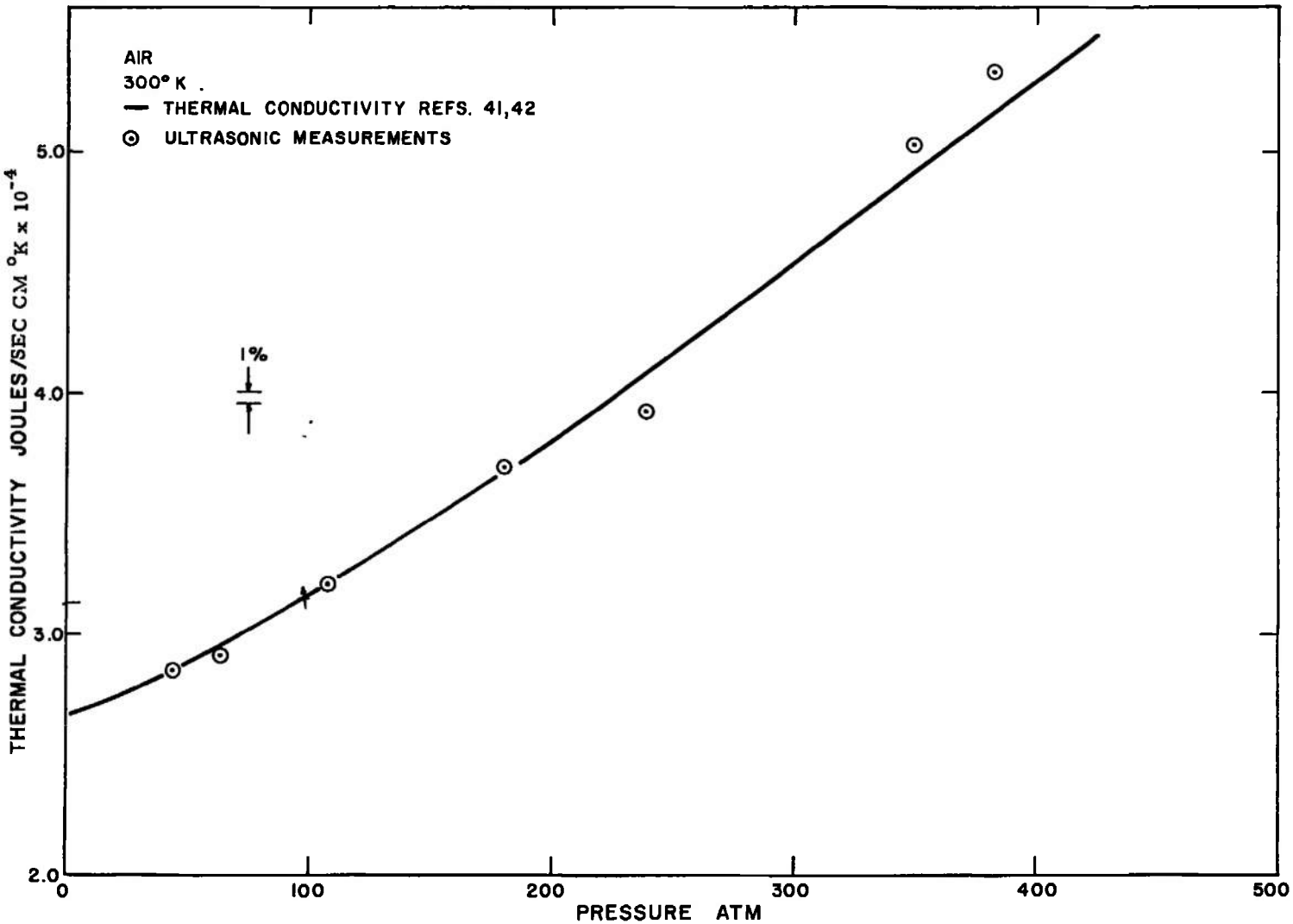

Fig. 16. Thermal conductivity of air versus pressure

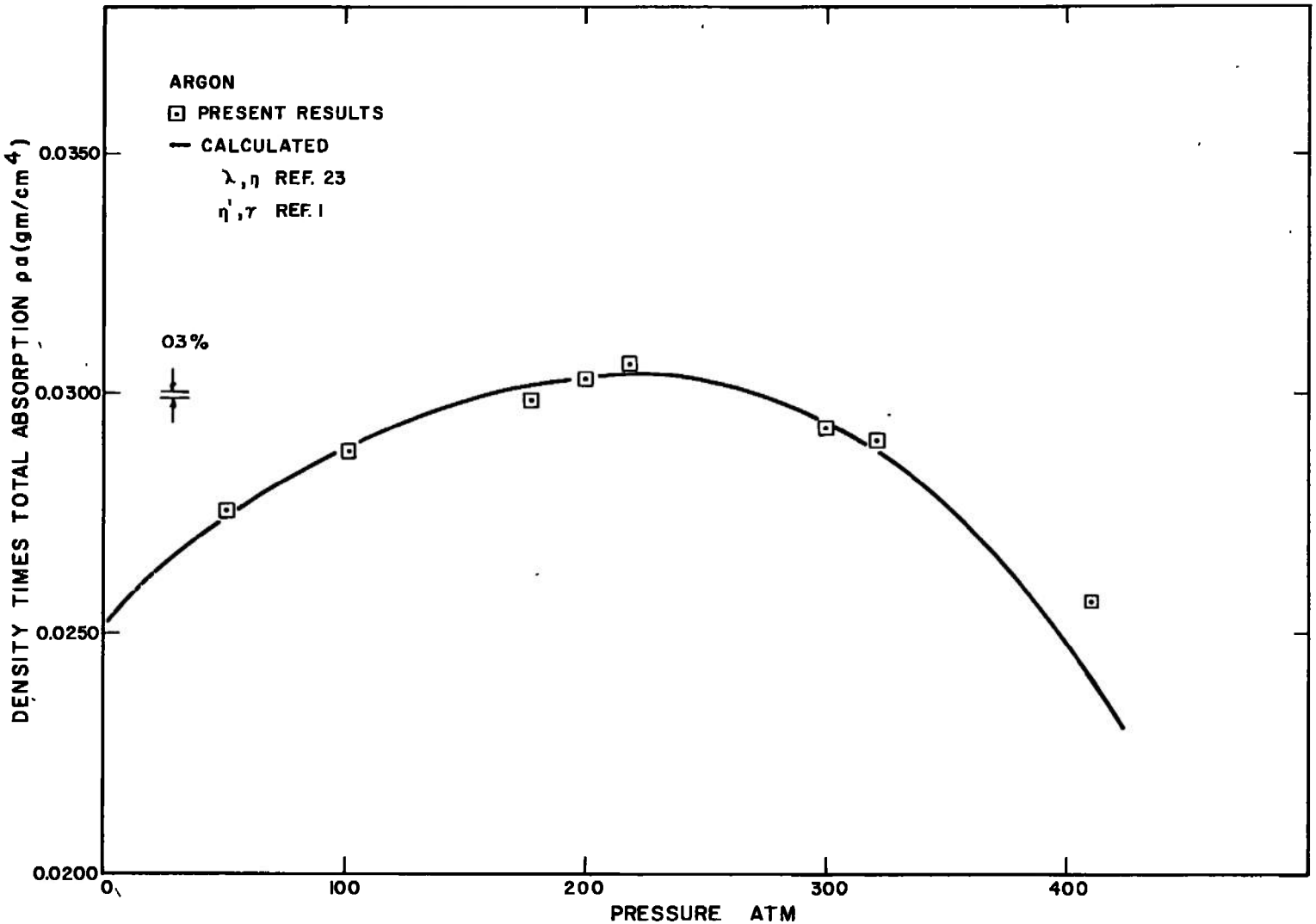

Fig. 17. Sound absorption versus pressure for argon by the pulse echo technique

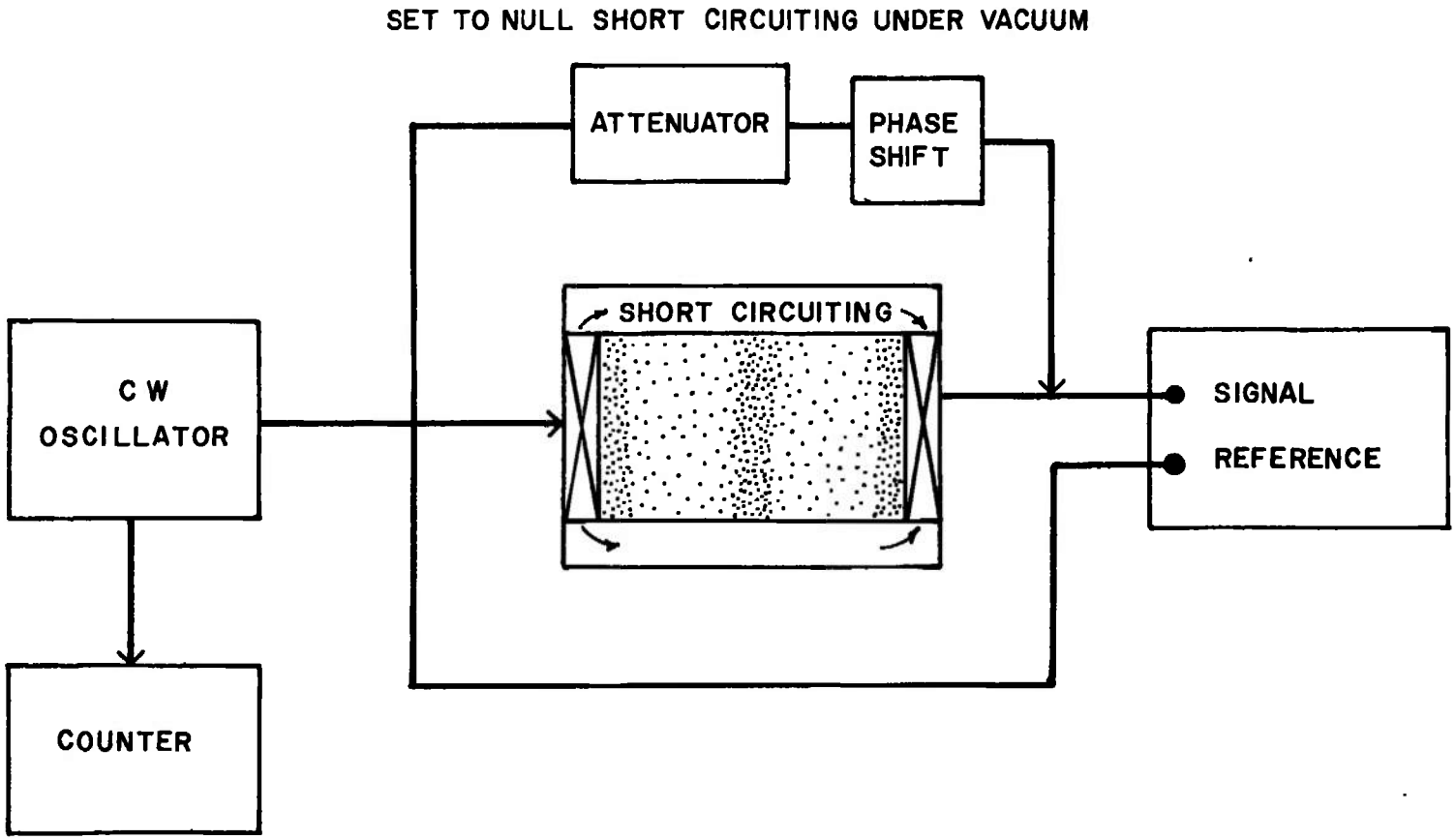

Fig. 18. Diagram of apparatus for acoustic cavity technique

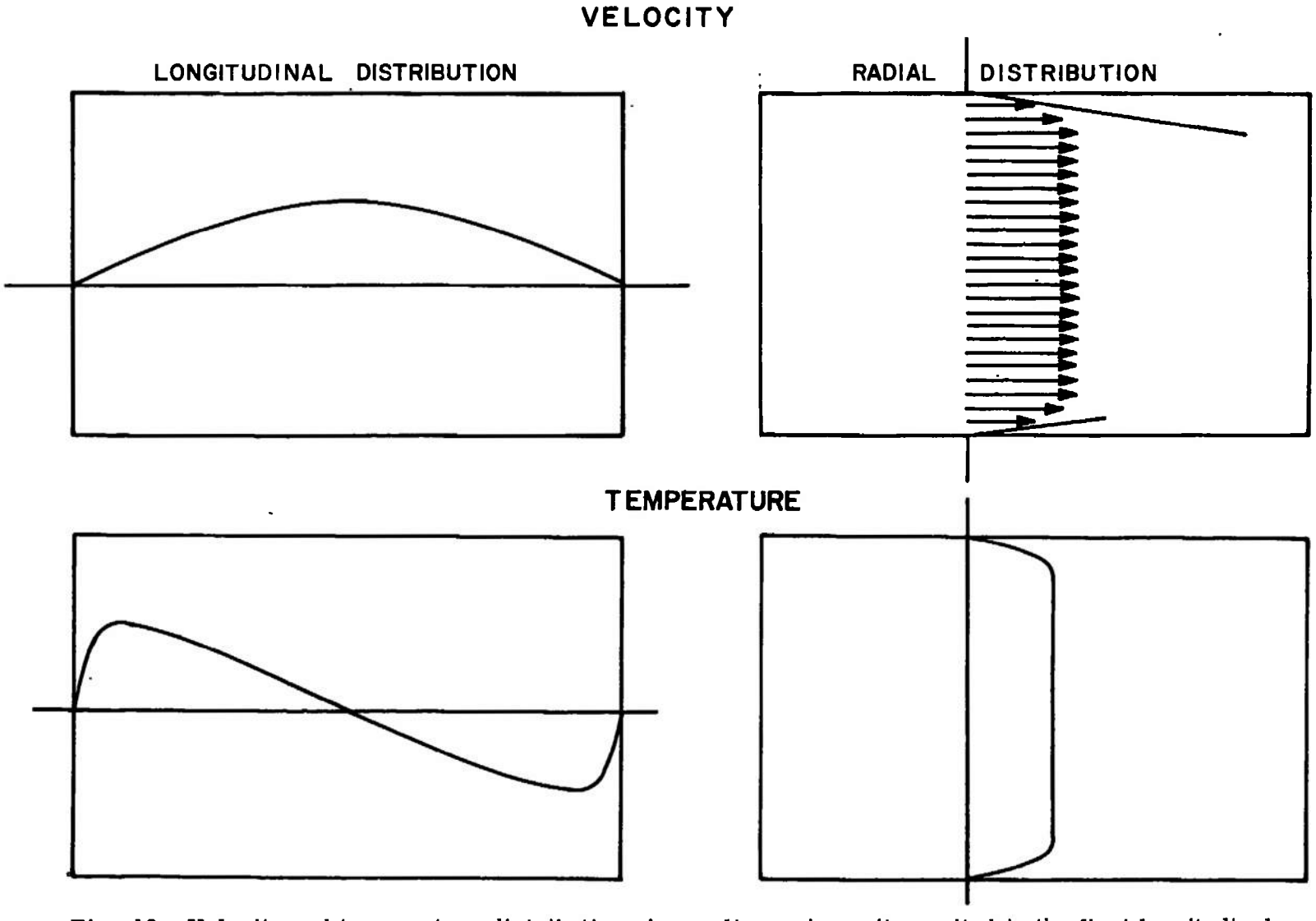

Fig. 19. Velocity and temperature distributions in an ultrasonic cavity excited in the first longitudinal mode

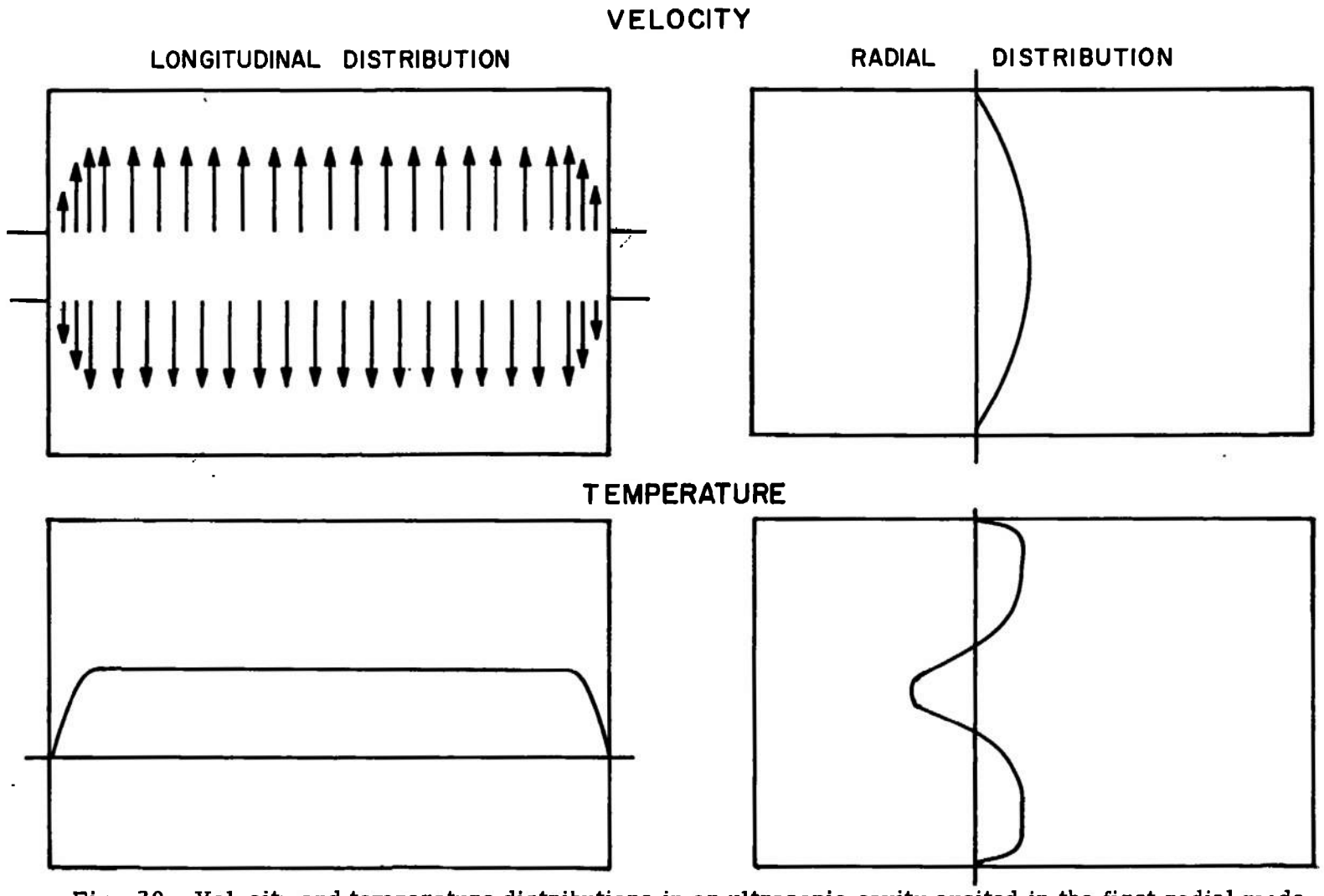

Fig. 20. Velocity and temperature distributions in an ultrasonic cavity excited in the first radial mode

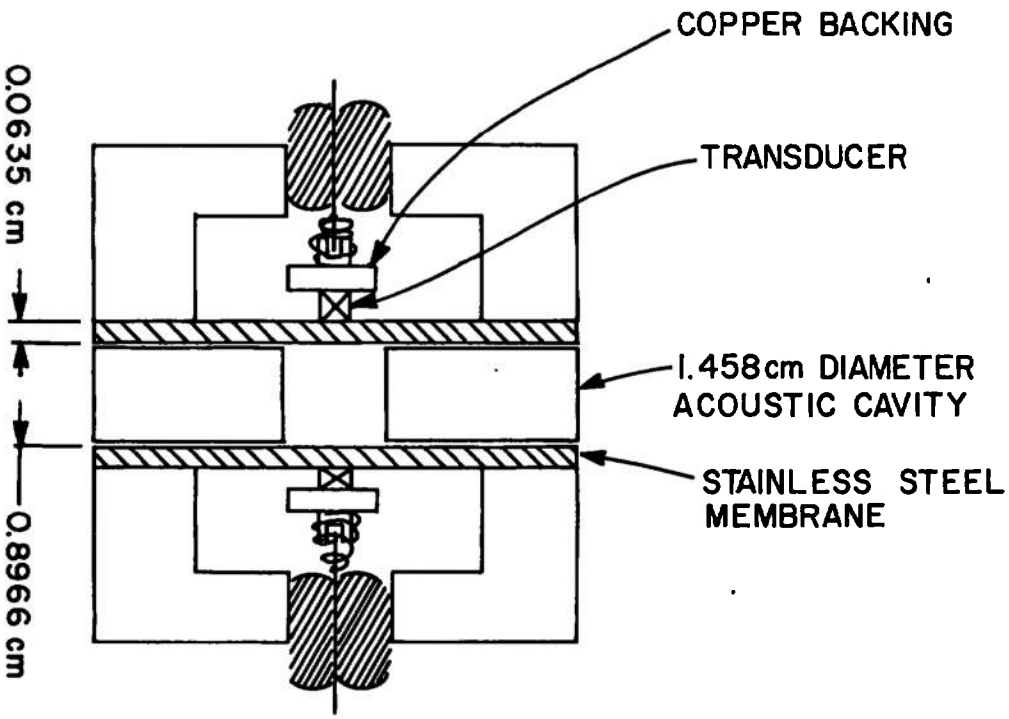

Fig. 21. Details of acoustic cavity used in initial transport property measurement with the cavity technique

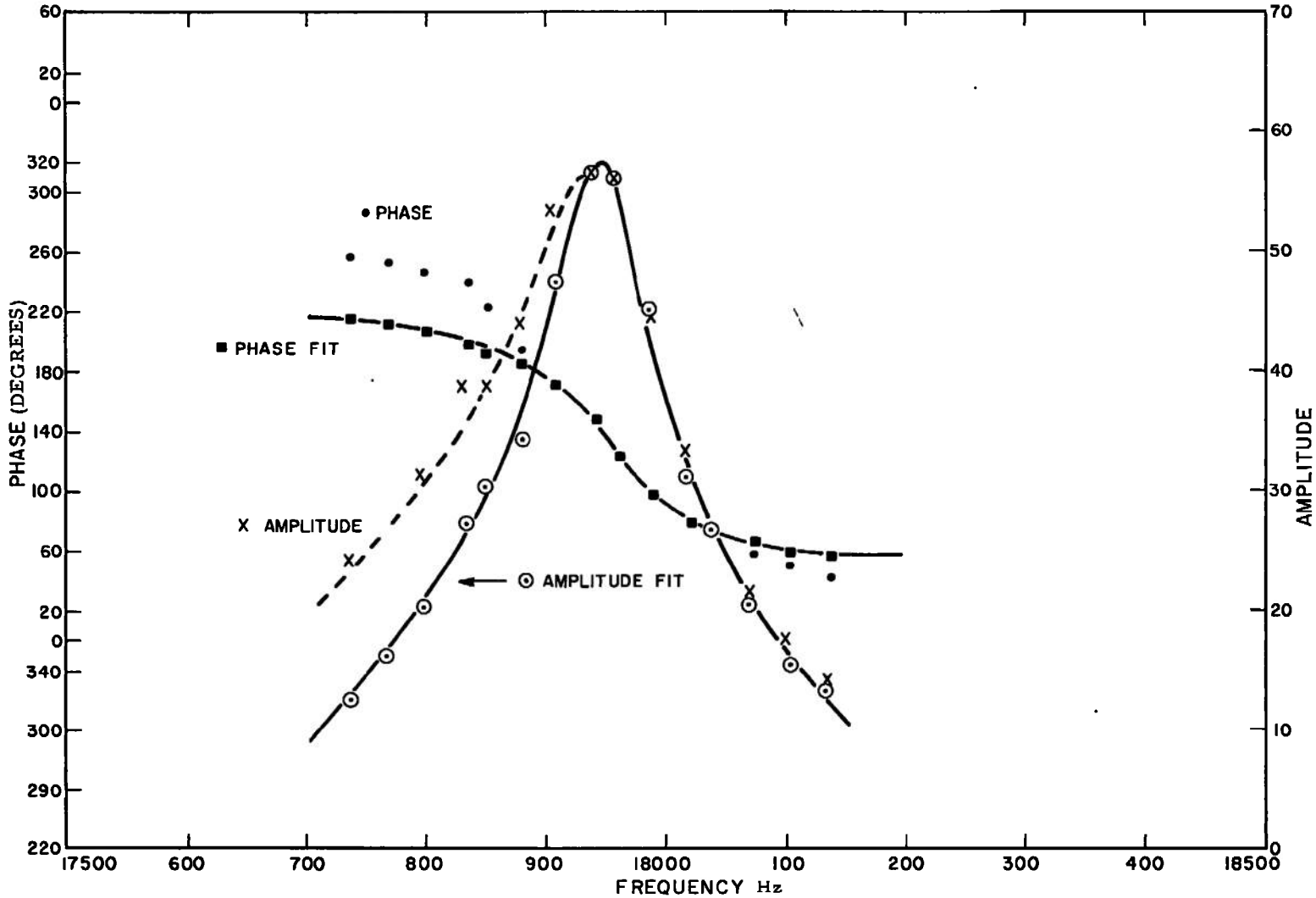

Fig. 22. Linewidth and phase shift for the first longitudinal mode

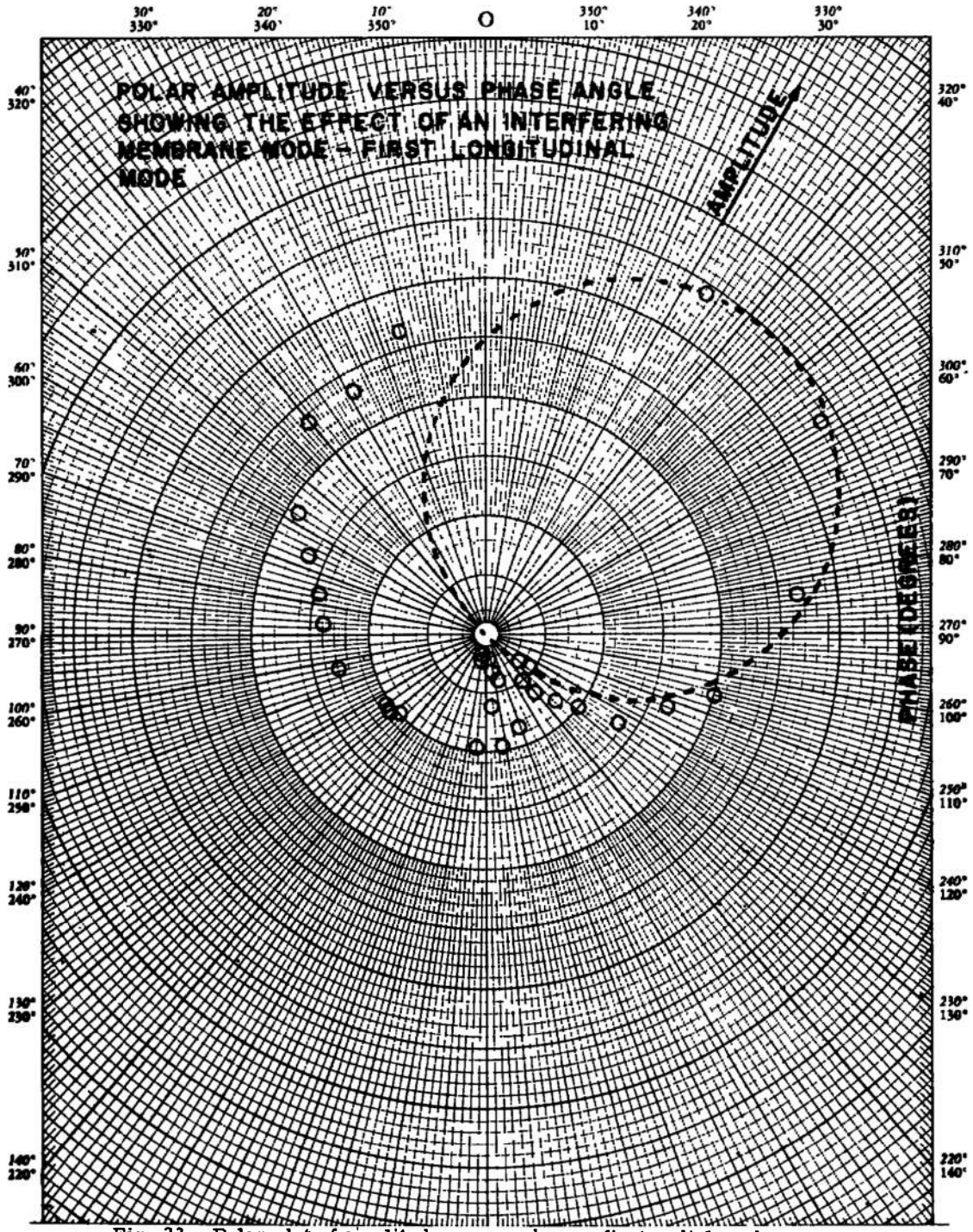

Fig. 23. Polar plot of amplitude versus phase - first radial mode

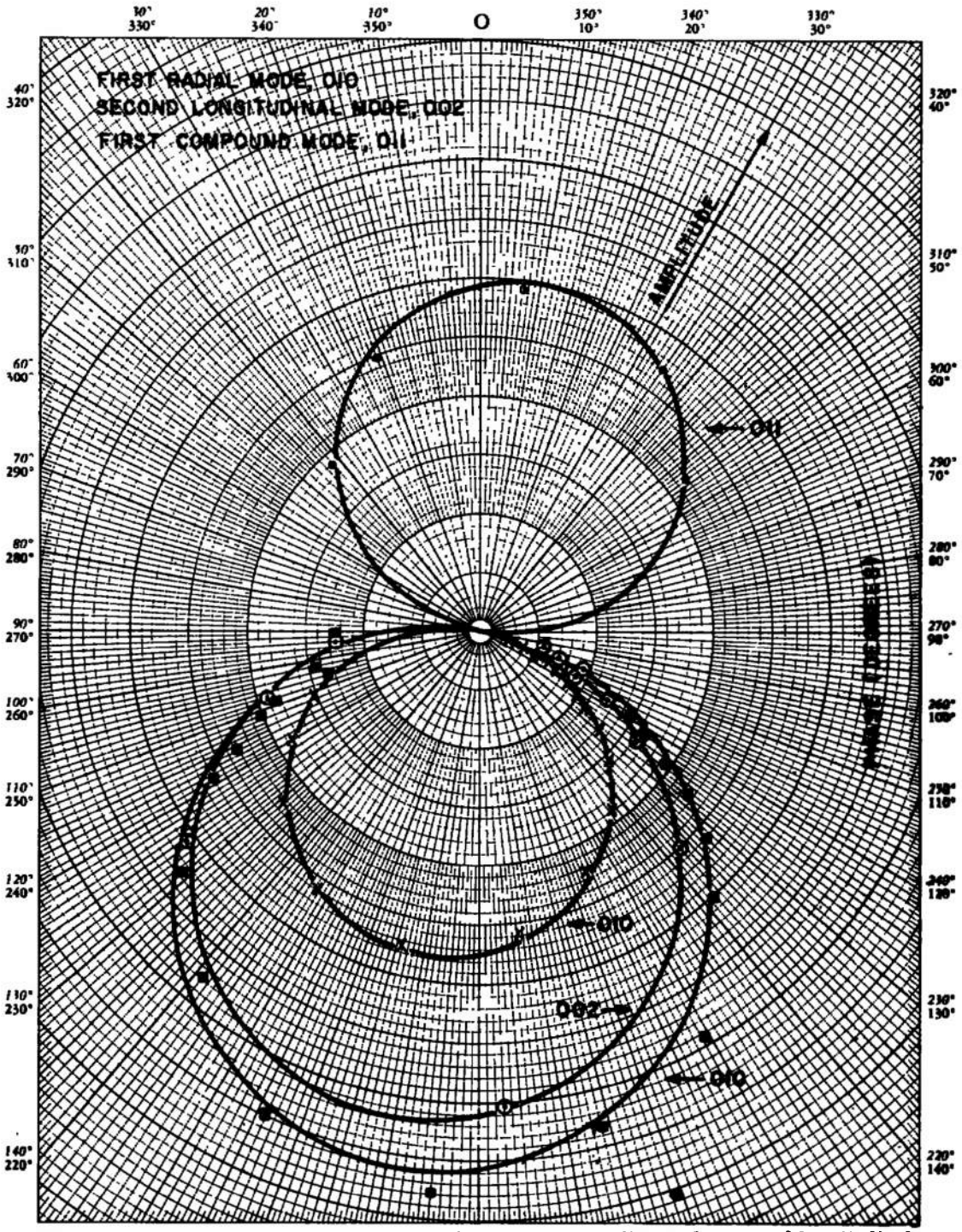

Fig. 24. Polar plot of amplitude versus phase for first radial mode; second longitudinal mode and first compound mode.

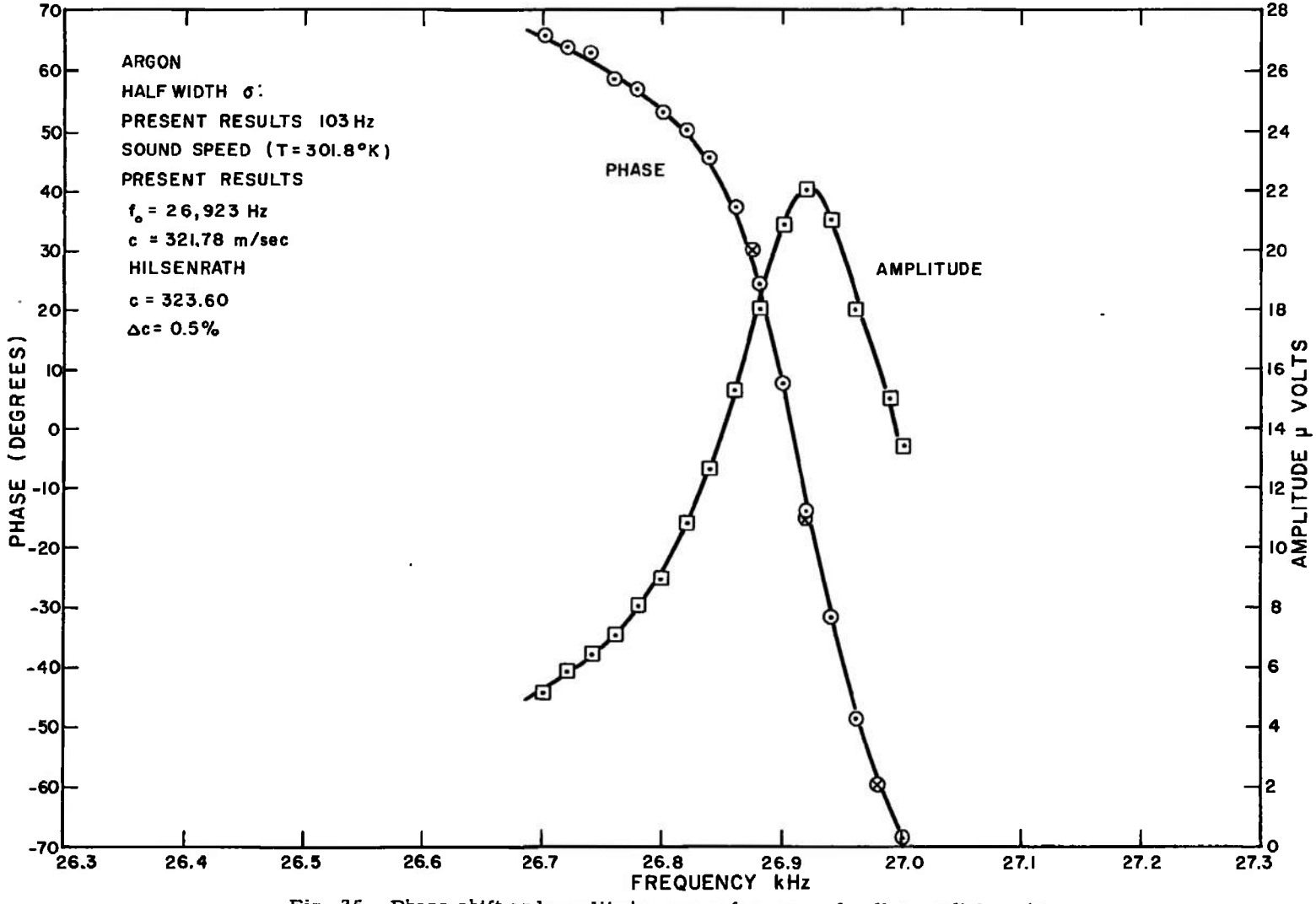

Fig. 25. Phase shift and amplitude versus frequency for first radial mode

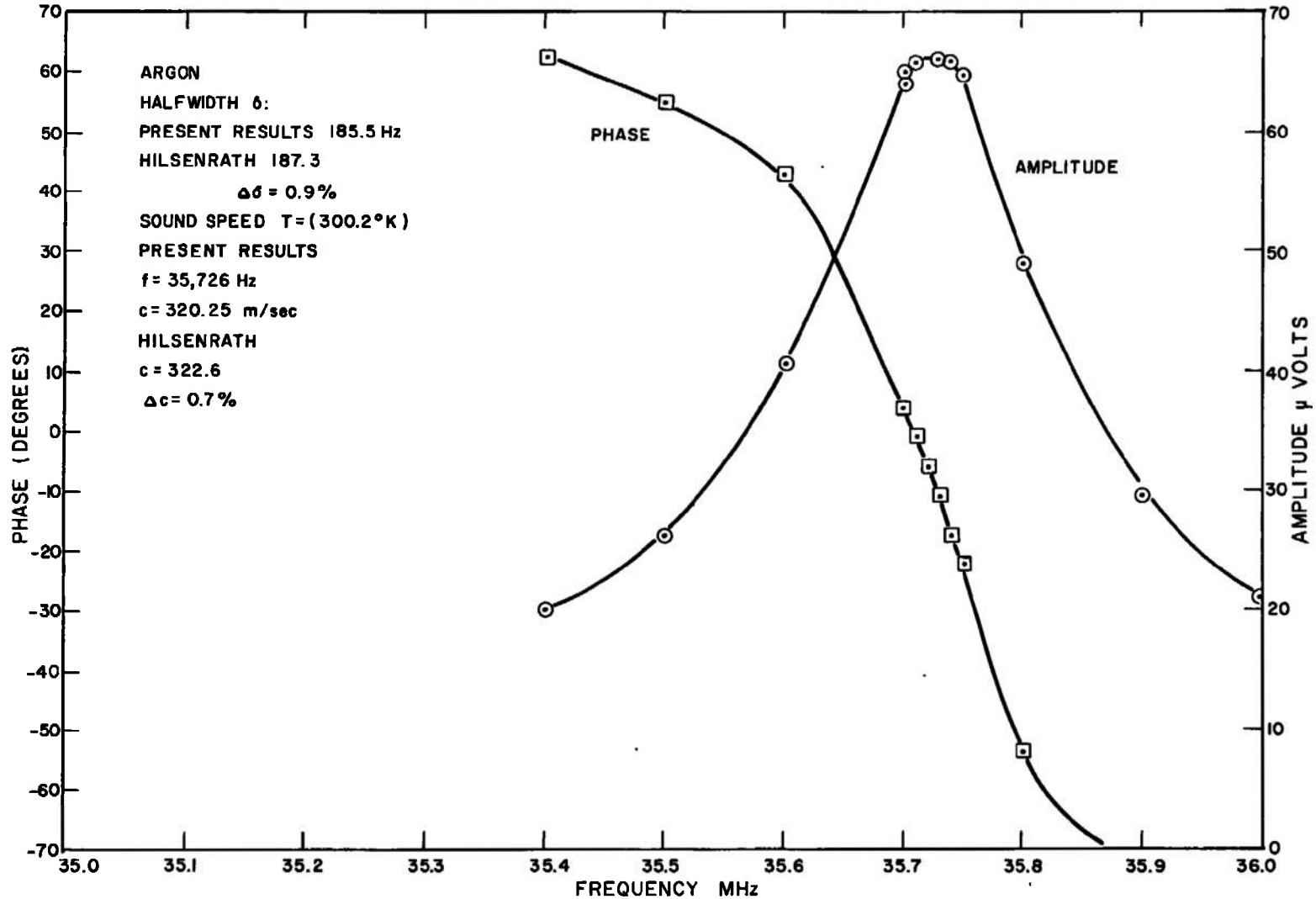

Fig. 26. Phase shift and amplitude versus frequency for second longitudinal mode

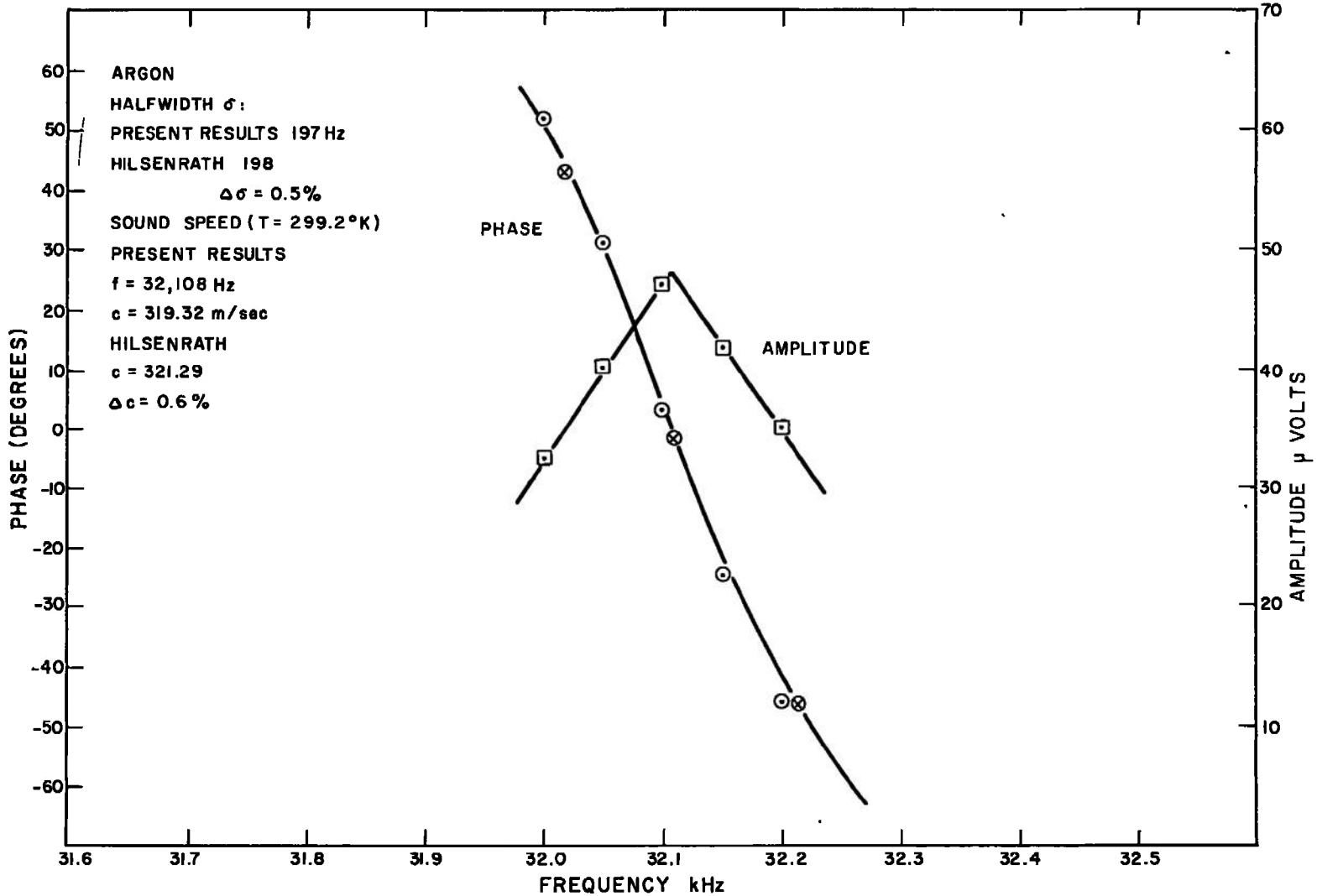

Fig. 27. Phase shift and amplitude versus frequency for first compound mode

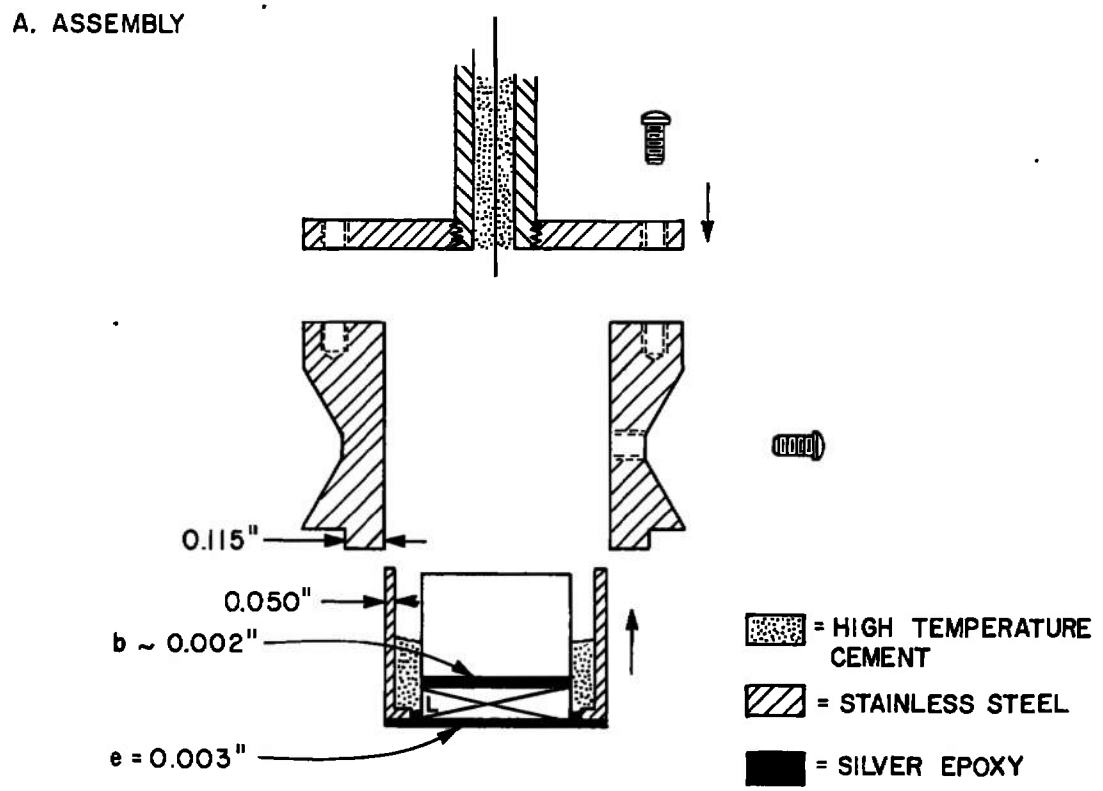

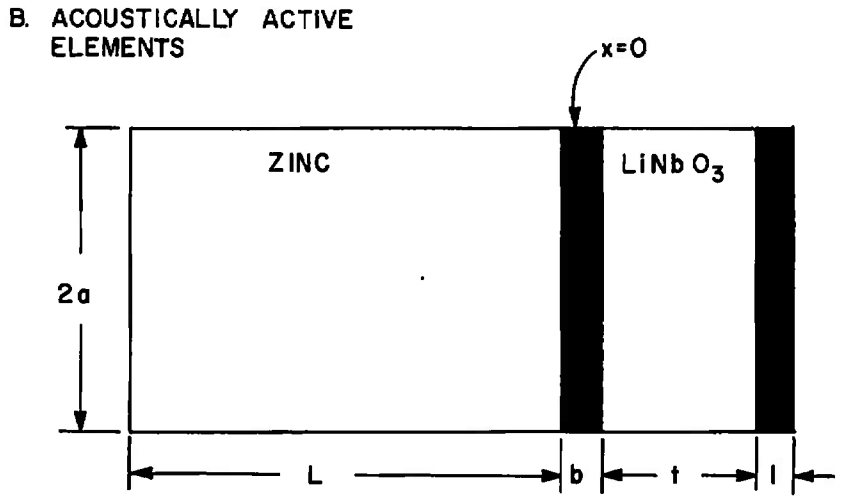

Fig. 1B. Details of transducer assembly for pulse techniques

UNCLASSIFIED

Security Classification

DOCUMENT CONTROL DATA - R & D

(Security classification of title, body of abstract and indexing annotation must be entered when the overall report is classified)

1. ORIGINATING ACTIVITY (Corporate author)
Panametrics, Inc.
Waltham, Massachusetts

2a. REPORT SECURITY CLASSIFICATION
UNCLASSIFIED

2b. GROUP
N/A

3. REPORT TITLE
RESEARCH STUDY AND EXPERIMENTAL PROGRAM TO DETERMINE THE TRANSPORT PROPERTIES OF HIGH TEMPERATURE AND HIGH DENSITY GASES

4. DESCRIPTIVE NOTES (Type of report and inclusive dates)
Interim Report - September 1968 to September 1970

5. AUTHOR(S) (First name, middle initial, last name)
C. Carey, J. Bradshaw, and E. H. Carnevale

6. REPORT DATE	7a. TOTAL NO. OF PAGES	7b. NO. OF REFS
September 1971	81	44

8a. CONTRACT OR GRANT NO.	9a. ORIGINATOR'S REPORT NUMBER(S)
F40600-69-C-0004 b. PROJECT NO. 8951 c. Program Element 61102F d. Task 895102	AEDC-TR-71-191 9b. OTHER REPORT NO(S) (Any other numbers that may be assigned this report) N/A

10. DISTRIBUTION STATEMENT
Approved for public release; distribution unlimited.

11 SUPPLEMENTARY NOTES	12. SPONSORING MILITARY ACTIVITY
Available in DDC	Arnold Engineering Development Center, Air Force Systems Command, Arnold AF Station, Tennessee 37389

13. ABSTRACT Transport property measurements with ultrasonic techniques are discussed over the entire temperature (100-15,000°K) and pressure (1-1000 atm) ranges. A chart of various techniques for the determination of transport properties in the various temperature and pressure ranges is given. Sound absorption and sound speed determinations were used to obtain thermophysical properties of argon, helium, nitrogen and air at room temperature and pressures between 1-500 atm. Several variations of pulsed ultrasonic techniques were used to obtain maximum precision in the gas property measurements. Sound speeds accurate to approximately 0.1 % were obtained in all the gases. Thermal conductivity and specific heat ratios were deduced for air. A cavity technique was developed for high accuracy (<0.1 %) viscosity, thermal conductivity and bulk viscosity determinations. Initial tests were run to proof the technique at room temperature and pressure. Sound speed, Prandtl number and viscosity measurements were made which agree with accepted values to within 1 %.

DD FORM 1 NOV 65 1473

UNCLASSIFIED

Security Classification

14. KEY WORDS	LINK A		LINK B		LINK C	
	ROLE	WT	ROLE	WT	ROLE	WT
gases						
transport properties						
high temperature						
high pressure						
high density						
ultrasonic tests						
thermodynamic properties						
electrical conductivity						
argon						
helium						
nitrogen						
air						

AFSC
Arnold AFS Tenn